Short-term Extreme Mooring Loads Prediction and Fatigue Damage Evaluation for Station-Keeping Trials in Ice

Chana Sinsabvarodom [a]*, Bernt J. Leira[a], Wei Chai[b]*, Arvid Naess[c]

[a]Department of Marine Technology, Norwegian University of Science and Technology

[b] School of Naval Architecture, Ocean and Energy Power Engineering, Wuhan University of Technology, China

[c]Department of Mathematical Sciences, Norwegian University of Science and Technology

* Correspondence author: chana.sinsabvarodom@ntnu.no; chaiwei@whut.edu.cn

Abstract: Full-scale tests of station-keeping trials (SKT) in drifting ice were conducted as part of research activities undertaken by the company Equinor in the Bay of Bothnia in March, 2017. In the SKT project, *Magne Viking* was employed as a moored supply vessel in order to measure the real-time loading during the full-scale tests. At the same time, *Tor Viking* was served as an ice breaker to maintain the physical ice management activities with different physical schemes i.e., the square updrift pattern, the round circle pattern, the circular updrift pattern and the linear updrift pattern. In this work, the ice resistance method is adopted to estimate the ice load during the full-scale experiment of station-keeping vessel in drifting ice. Extreme mooring loads and accumulated fatigue damage corresponding to different ice management schemes are considered based on the full-scale measurements. As a result, the ice resistance method can be directly applied to predict the (undisturbed) mooring loads for station-keeping of ships in ice without being influenced by the effect of different ice management operations. Moreover, for estimation of the statistical properties of the extreme mooring load, the block maxima method, the peaks-over-threshold method, and the ACER method are applied for each of the ice management schemes. It is observed that predictions of the extreme mooring loads by the adopted procedures deviate by around twenty percent. Regarding the efficiency of the ice management schemes, it is assessed that the circular updrift pattern provides the best result. Furthermore, the Rainflow counting procedure are applied to evaluate the fatigue damage of the mooring line for the difference ice management schemes. Regarding the degree of fatigue degradation, application of the circular updrift pattern for the purpose of ice management is seen to imply the lowest damage level.

Keywords: station-keeping trials; Ice loads; extreme ice load, fatigue assessment

NOMENCLATURE

ACER	*Average conditional extreme rate*
ADCP	*Acoustic Doppler current profiler*
BM	*Block maxima*
COV	*Coefficient of Variation*
DB	*Drift Beacon*
DPAM	*Dynamic positioning assisted mooring*
EV	*Extreme Value*
MBL	*Minimum breaking load*
IM	*Ice management*

	IPS	*Ice profiling sensor*
1	**IPS**	*Ice profiling sensor*
2	**MV**	*Magne Viking*
3	**POT**	*Peaks over threshold*
4	**SKT**	*Station-keeping trials (in ice)*
5	**STD**	*Standard Deviation*
6	**SWL**	*Safe working load*
7	**TV**	*Tor Viking*
8	**ULS**	*Upward looking sonar*

1. Introduction

The number of offshore activities in waters exposed to sea ice has been increasing steadily during the last decades (Hahn et al., 2017). The stationary-keeping of ships and offshore structures in ice becomes very challenging because the loading on the mooring systems due to the sea ice is caused by the global ice loads which are highly uncertain since they are the result of sea ice properties and complex failure mechanisms. Understanding the behavior of the ice, the ship structure interaction as well as the dynamic responses of ships subjected to ice loads can improve the planning and design of ship operations. In turn, this has implications for safety, integrity, cost efficiency and regularity of ship operations (Kujala, 1996). There are several offshore activities that require the vessel to maintain its position during various operations, such as lifting, installation, crew change, evacuation, drilling, tanker loading, maintenance of subsea equipment , etc. (Gürtner et al., 2012). Structural health monitoring can be applied to perform reliability updating in order to enhance the safety and integrity of ships and offshore structures during operations in ice (Leira, 2016).

The global loading due to ship-ice interaction can be estimated by application of the ice resistance method based on the geometric shape parameters of the ship hull and the sea ice properties such as ice thickness, ice drift speed, ice density etc. (Erceg and Ehlers, 2017; Riska, 1997). The variability associated with these quantities gives rise to a corresponding variability of the ice resistance during the ship-ice interaction process (Wang et al., 2021).

The theory of extreme value can be applied to estimate the maximum ice loads corresponding to the operational return periods to cover all loading uncertainties (Chai et al., 2018b). A non-parametric probabilistic approach based on kernel density functions can also be applied to estimate the ice loading on ship for a given stationary condition. This provides good results especially for the upper tail of the short term peak distribution (Suyuthi et al., 2012a). However, extrapolation to long-term conditions with varying ice conditions becomes more difficult unless re-fitting of the density function for each short-term condition is performed.

In order to compute the extreme ice loads to be applied for design of the mooring system, a range of different short-term (stationary) environmental conditions would be considered. This would also apply to design of the ship hull in general (Kujala, 1996; Li et al., 2021). These short-term conditions would depend both on the ice environment and the operational profile of the ship (i.e. the criteria defining the maximum ice thickness in which to operate).

For the purpose of "weighting" the extreme mooring line forces during these conditions according to their likelihood of occurring, a formulation based on conditional short term extreme value distributions would be highly relevant. The statistical parameters of the short-

term distributions would then be functions of the ice environment and the operational parameters (Chai et al., 2021; Wang et al., 2021). A similar conditional formulation for the probability distribution of the stress cycles in the mooring line could be achieved.

Unmanaged drifting sea ice can thus generate long-term extreme ice loads which are beyond the capacity of the station-keeping system. This may cause failure of the mooring system, the dynamic positioning (DP), ship structure, operation equipment, etc. In order to avoid this, ice manage schemes can be employed, e.g. by application of icebreakers working upstream relative to the system to be protected. Generally, a continuous channel of thoroughly broken-up ice floes is then created. This can reduce the ice loads e.g. on a stationary vessel into levels that can be tolerable (Hamilton et al., 2011). So far, only a limited amount of data from different full-scale testing scenarios for ice manage systems exists, and even less are publicly available (Liferov et al., 2018).

Metocean ice data for the purpose of ice management planning can be obtained based on several types of ice observations implemented on different types of sensor platforms, i.e. airborne (Satellites, etc.), surface-based (shipboard, camera, buoys, GPS, etc.) and subsea (IPS, ULS, ADCP, et) (Haugen et al., 2011). Especially in areas with icebergs, more data related to metocean ice condition is required because physical ice management has to consider both ice breaking and iceberg management. For some ice conditions, icebergs might also drift together with the sea ice towards the structure during the operations. The characteristics of broken ice in the iceberg drift must be investigated for the purpose of planning the ice management operation (Yulmetov et al., 2016). Furthermore, broken ice and icebergs have different motion characteristics due to the difference in mass, inertia and momentum.

In order to obtain more relevant data, the company Equinor (Statoil) conducted full-scale testing based on station keeping trials (SKT) in ice in the Bay of Bothnia in March 2017. The anchor handling tug supply vessel performed station keeping operations during various ice conditions, including managed and non-managed ice. Trial physical ice management has been performed by the icebreaker to investigate the performances of ice management operations under different conditions. An overview of the SKT project is given in Liferov et al. (2018). As a preparation of the full-scale station keeping tests for the relevant ice condition, a simulation of the ice-structure interaction was performed by means of the Aker Arctic Ice Management Suite (AIMS) program (Neville et al., 2016). The IM operation were planned in advanced and executed in such a way that the target ice conditions required for the station keeping test. During the full-scale experiment, relevant data was collected. This provides a great opportunity to calibrate the numerical ice management analysis tool. Furthermore, simulation of the IM operations was also conducted by application of the Equinor computer program "Simulation of Interaction between Broken Ice and Structures (SIBIS)" in order to validate the software and to enhance the accuracy of the simulation. The SIBIS program performs the time domain simulation of the interaction process between the broken ice and the structure (Serre et al., 2018).

For design of mooring systems, both overloading due to extreme environmental conditions as well as accumulated fatigue damage must be considered. For temporary operations, only analysis for the extreme response is required (API, 1996). Typically, mooring system design is based on the limit state approach. The probability of overloading the mooring systems can be estimated based on the prediction of extreme values corresponding to a specified return period

(reflecting the anticipated time in operation)(Veritas, 2010). The standard ISO 19906 also allows the design approach to be based on full-scale experiments in order to quantify representative ice actions. The design parameters obtained from the full-scale measurement can be applied to both physical models and mathematical models in order to estimate the ice loads by taking into account the uncertainties corresponding to the application (ISO, 2010). For permanent operations, accumulation of fatigue in the mooring lines has to be quantified when the mooring system is positioned at the same location for five years or more (API, 1996). Typically, the fatigue capacity of the mooring system depends on that of its components such as chain, wire rope, fiber rope, connecting links etc. This capacity can be represented in terms of TN or SN curves (API, 1996; Veritas, 2010).

For the ice management system, the most efficient way to generate a channel of uniformly reduced floe sizes in drifting ice is to operate the icebreaker in systematic patterns such as a circular form, an elliptical form, a racetrack form, an orbital form, a linear form etc. The icebreaker can operate in the updrift direction in order to protect the stationary vessel. The main factors influencing selection of the pattern to be applied for the icebreaker are the ice drift speed, the ice thickness, the turning rate of the incoming ice and the maneuvering capability of the icebreaker. Two or more icebreakers can be employed with the same pattern to enhance the efficiency of floe size reduction (Hamilton et al., 2011). Fenz et al. (2018) studied full-scale measurement obtained during station-keeping in managed ice in the area North of Svalbard. It was found that the local pressures measured during the tests resulted in design curves for the ice pressure that were reduced corresponding to vessel transit through unbroken ice.

The objectives of the present paper are to identify the most relevant types of short-term extreme value and cycle distributions based on available measurements. As the next step in order to provide values for application to design of a particular mooring system, the variation of the statistical parameters of these distributions as functions of the long-term ice environment and the operational parameters would need to be determined. This can be achieved through application of the formulations presented herein, but this scope is to wide to address in the present study. It is hence pointed to as a necessary extension to be addressed by future work.

The characteristics of the extreme mooring loads are presently estimated by using recorded data from the full-scale measurements during the station-keeping trials (SKT) in drifting ice. The different management schemes under different ice condition are considered. Three procedures are applied for investigating the extreme mooring loads: the block maxima method (BM), the peaks-over-threshold method (POT) and the ACER method. Extrapolation to long-term extreme loads is studied. The accumulated short-term fatigue damage of the mooring line for each of the ice management schemes is also considered.


2. **Ice management operations**

2.1 Overview of vessels for ice management operations.

Ice management systems are typically employed during operation of ships and floating structures in ice cover areas in order to reduce the ice loading (El Bakkay et al., 2014; Hamilton et al., 2011). During the present experiments, the icebreaker was deployed in order to cut the

ice according to different ice manage schemes. Selection of vessel types and equipment to be applied in the field experiments were based previous experience with complex marine operations for similar conditions. Two vessels are involved in the experiments i.e., one ice-breaking vessel and one stationary supply vessel. Both vessels have previously been operating under both Arctic and Baltic ice conditions., and both vessels have a diesel mechanical shaft line system. The propellers of the vessels are nozzle mounted. The shaft generator of the vessels provide power to electrical tunnel thrusters and retractable azimuthon thrusters in the bow (Kjøl et al., 2018). MV is a standard offshore vessel with a bulbous blunt shape as illustrated in figure 1. The bow shape of the vessel TV is optimized with respect to icebreaking and ramming as illustrated in figure 2. The vessel characteristics of TV and MV are listed in Table 1.
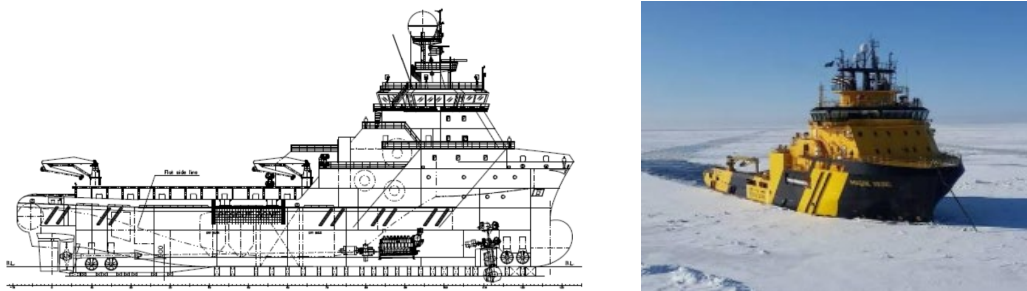
Figure 1. Drawing Arrangement and photo of Magne Viking
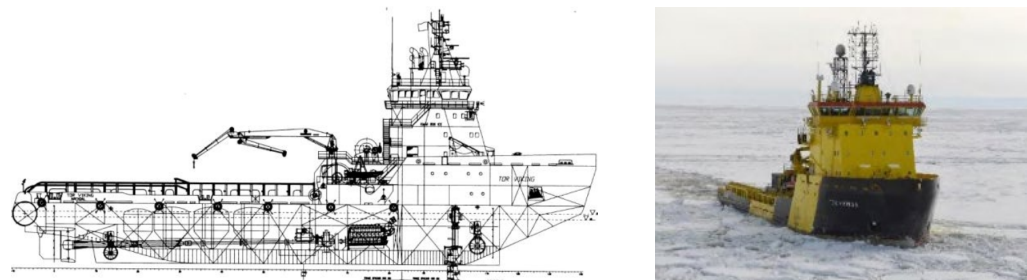
Figure 2. Drawing Arrangement and photo of Tor Viking

Table 1: The main characteristics of Tor Viking, TV, and Magne Viking, MV (Kjøl et al., 2018)

Item	Magne Viking	Tor Viking
Built Year	(Astilleros Zamakona) 2011	(Kværner Leirvik) 2000
Ice Class	DNV 1A (FSICR) 80 cm	Icebreaker ICE-10 (1m)
Level Ice Breaking Capacity (600kPa)	Approx. 50 cm at 7.5 knots	Approx. 50 cm at 13 knots
Maximum Speed in Open Water	17.5 knots	16 knots
Length Over All	85.2 m	83.7m
Beam	22m	18 m
Max Draft at Summer mark	7.6 m (+92 cm for skeg)	7.24 m
Displacement at Summer Draft	9971 T	6800 T

|		
Light Ship weight	5670 T	4357 T
Deadweight at Summer draft	4301 T	2366 T
Gross Tonnage	6279	3382
Bollard pull	251 T	200 T
Total BHP	19050	18300
Propulsion	2x7 MW CPP (Nozzle)	2x6,7 MW CPP (Nozzle)
Tunnel Thrusters/Azimuth	4x830 kW/l x 830 kW	2 x 880 kW/1 x 880 kW
Anchor Handling Winch	IP Huse 400T/5 Drum	IP Huse 400T/4 Drum

1

2.2 Ice breaker deployment patterns for ice management.

The main purpose of ice management operations is to reduce the ice load on the vessels in order to remain on station such that offshore operations can be properly conducted. The most efficient way to reduce the ice load on the vessel is to create a uniform channel in order to decrease the floe sizes of the moving ice by means of an icebreaker moving according to systematic patterns (Hamilton et al., 2011). For optimum performance, the shape of the patterns can be altered depending on the speed, thickness and turning rate of the incoming ice, the maneuvering capability of the ice breaker etc.
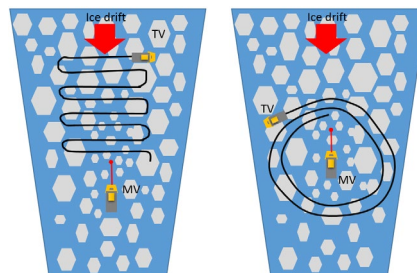
(a) Case 1: Square updrift tracks   (b) Case 2: Round circular tracks

(c) Case 3: Circular updrift tracks   (d) Case 4: Linear updrift tracks

Figure 3. Patterns corresponding to the different ice management schemes applied during full-scale tests

 Four different ice management schemes were applied during the full-scale trials as illustrated in figure 3. The corresponding measurement records are presently analyzed in order to estimate the statistical properties of the extreme mooring forces. The selected ice management patterns were achieved by using the ship's electronic chart display and information system (ECDIS) to

plan the route of the ice breaker. ECDIS is of particular advantage during periods with low visibility (Neville et al., 2018). The most challenge part of the ice management operation is during the initiating pattern, mainly since the ice is unbroken at this stage. The speed of the vessel was accordingly relatively low during the first turn. Hence, it takes a relatively long time in order to make the first pass compared to subsequent passes.

The first ice manage scheme corresponds to the square updrift pattern as illustrated in figure 3a, with straight-line crosscutting of the sea ice in the updrift direction. The square updrift pattern allows the icebreaker to increase the speed along a straight-line before making sharp 90 degree turns at the transition points. However, the combination of high speeds and sharp turns associated with the square pattern can cause excessive roll of the vessel. The second pattern is the round circular track. The icebreaker will travel around the supply vessel as illustrated in the figure 3b, which is suitable for low drift speeds in order to minimize the outgoing floe size and produce a large quantity of brash. The third pattern corresponds to circular updrift tracks as illustrated in figure 3c. For this scheme it is relatively easy to push the ice into the previous track. Consequently, there is a significant reduction of the turning resistance. Relatively high speeds of the icebreaker, typically about 10-12 knots, were achieved after the ice management was initialized. The circular approach is the most effective and preferable for most of the ice conditions encountered during the trials, except when the ice drift speed was relatively high and the ice conditions were relatively severe (Neville et al., 2018; Sinsabvarodom et al., 2020b). The last pattern corresponds to the linear updrift track. This represents a novel IM scheme that was implemented as part of the station-keeping trials.

The time table of the different tests is listed in table 2. The schedule in the time table is slightly different from that established during the mission planning. The time schedule in table 2 is based on the start and the completion of the real time records from the IM operations.

Table 2- The schedule for the different IM operations

| Ice management operation	Date	Time
Square updrift pattern	9-Mar 2017	11:00:00 –13:15:00
Round circular pattern	12-Mar 2017	10:00:00 –14:25:00
Circular updrift pattern	16-Mar 2017	19:40:00 –21:40:00
Linear updrift pattern	16-Mar 2017	21:40:00 –00:30:00

2.3 Weather Conditions

During the field experiment, the met-ocean conditions such as air-temperature, wind speed, wind direction, ice draft, ice drift speed, ice concentration, etc., were recorded. Underwater ice profiler sensors (IPS) were installed and moored to the seabed as illustrated in figure 4b. The location of the IPS are listed in Table 3 and the geographical location of the ice profilers in the Bay of Bothnia are shown in figure 4a. Further details in relation to the IPS stations are given in Teigen et al. (2018). The IPS were located approximately 35-35 m below the water surface

so as to measure the draft of the sea ice as illustrated in figure 4b. Acoustic Doppler Current profilers (ADCP) are deployed in order to measure the ice drift speed and direction. Furthermore, ice drift beacons were also deployed on the surface of the ice in order to monitor the ice drift velocity as illustrated in figure 4c.

(a)   (b)   (c)
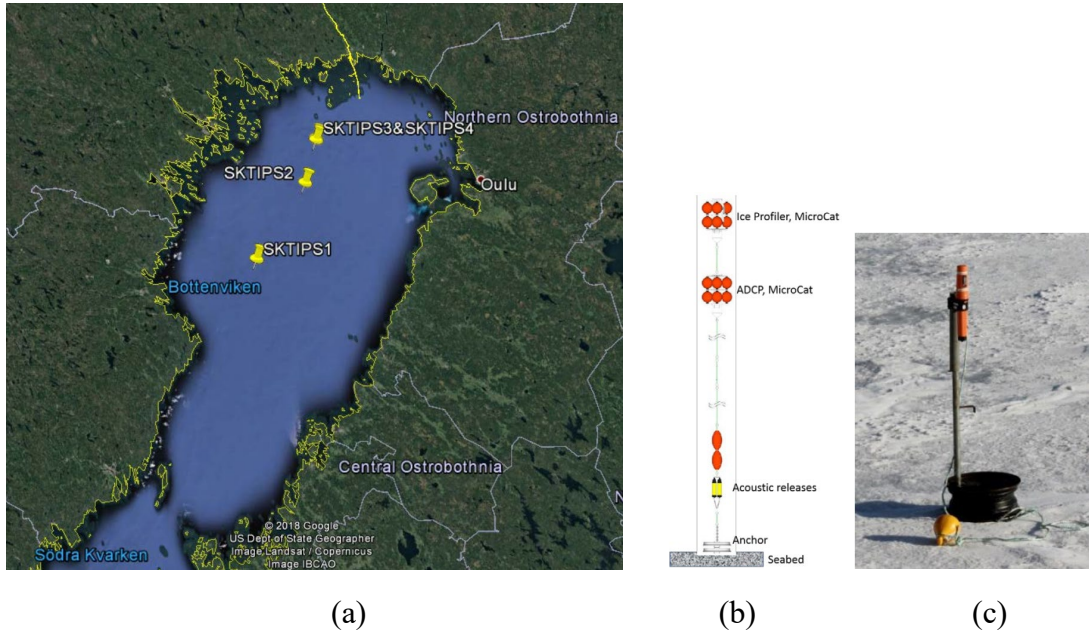
Figure 4: a) The geographical locations of the ice profilers in the Bay of Bothnia, b) Ice profiler stations (IPS), c) Ice drift beacon (DB) (Teigen et al., 2018)

Table 3- Relevant characteristics for the different IM operations

Stations	Latitude	Longitude	Deployed	Recovered	Duration	Depth
IPS 1	64º46.483'N	22º24.492'E	2017/03/07 10:16:07	2017/03/10 10:16:57	72 h	85 m
IPS 2	65º07.959'N	23º11.230'E	2017/03/11 12:56:20	2017/03/13 15:56:04	50 h	104 m
IPS 3	65º21.491'N	23º22.230'E	2017/03/15 14:59:22	2017/03/17 08:18:17	42 h	64 m
IPS 4	65º20.943'N	23º25.629'E	2017/03/15 15:38:48	2017/03/16 15:45:28	24 h	64 m

During the full-scale experiments, the sea ice in the Gulf of Bothnia was generally drifting from the West to the North directions, which can be observed from daily satellite's images as

illustrated figure 5. However, on 8-10 and 12 March there were congested clouds across the sky, which prevented the satellite from taking photographs of the sea ice. Because of sea ice drifting from the West to the North direction, the full-scale experiment of the SKT project were also oriented in the same directions as illustrated by the ship tracks and the test locations of TV and MV in figure 6.
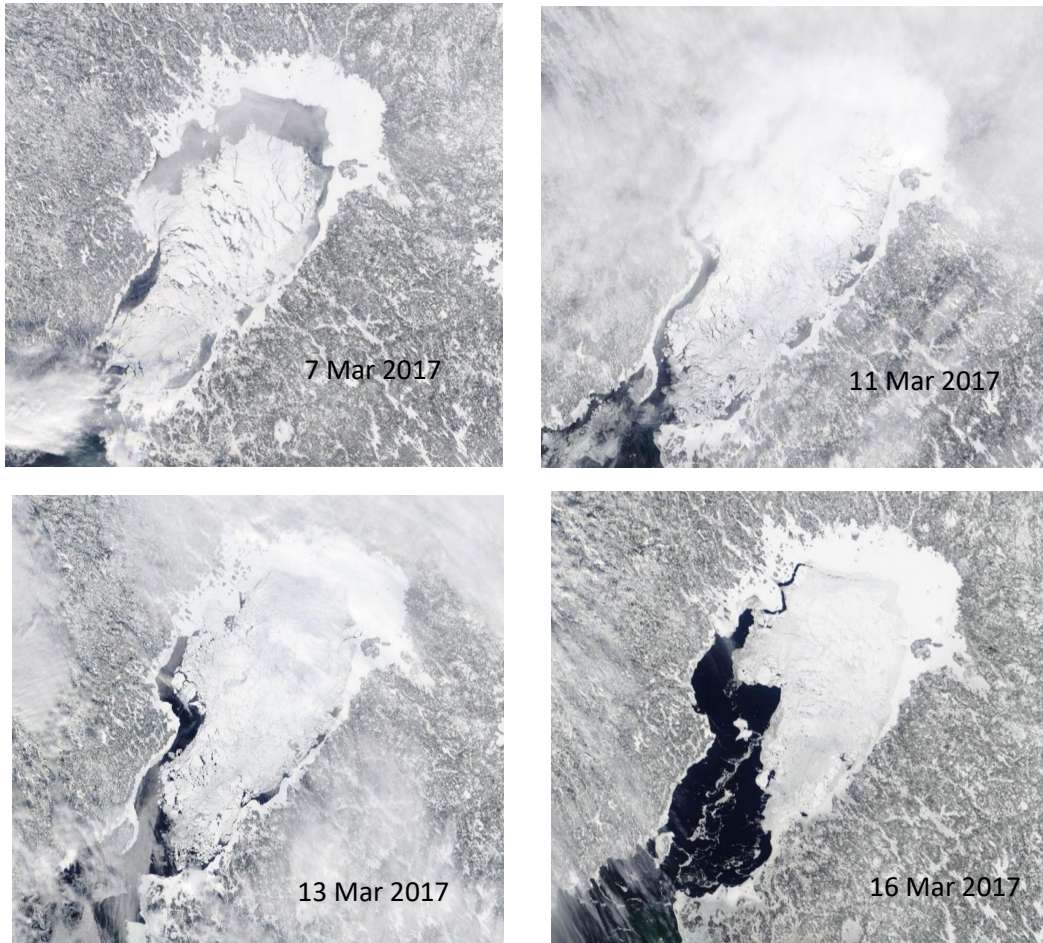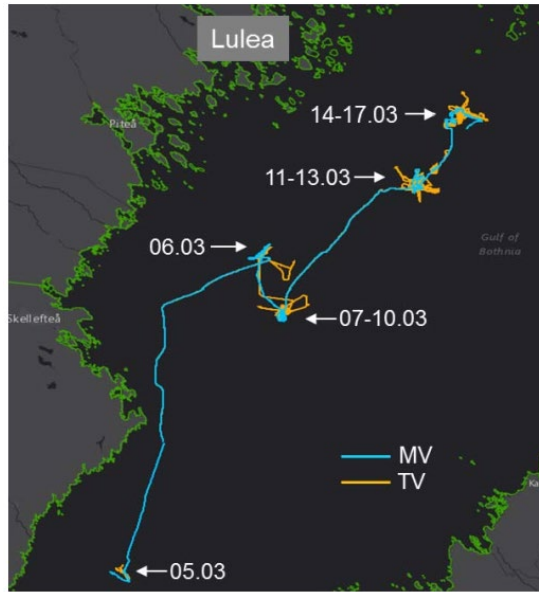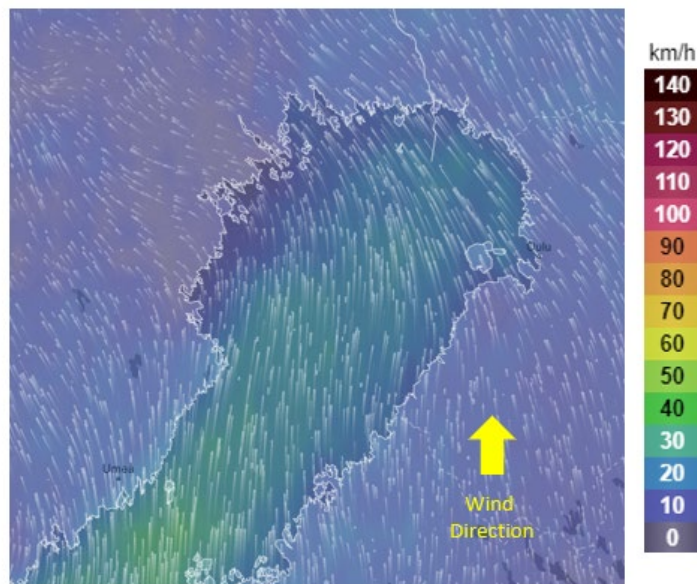

7 Mar 2017

11 Mar 2017

13 Mar 2017

16 Mar 2017

Figure 5. Satellite images during the field experiment (Source: https://zoom.earth)

(Remark: On 8-10 March and 12 March 2017 the sky was covered by clouds)

Figure 6. Ship tracks and test locations (Liferov et al., 2018).

Figure 7. An example of a geographical contour for the wind speed illustrated by the directional stream lines at 19:00 on 13 March 2017. (Source: www.ventusky.com)

Typically, the ice drift speed is approximately 1 to 2 percent of the wind speed (Spreen et al., 2011). During the experiment in the Bay of Bothnia, it was found that the ice drift speed was around 1.5 percent of the wind speed as illustrated in the figure 8. Typically, the sea ice drift direction on the Northern hemisphere deviates by 25 to 30 degrees relative to the wind at the surface (Leppäranta, 2011). This is reflected by the spikes in the wind and ice rose diagrams as illustrated in figure 9. The deviation angles between the wind and ice drift directions are due to ice-water drag, the Coriolis forces, etc. (Leppäranta, 2011).
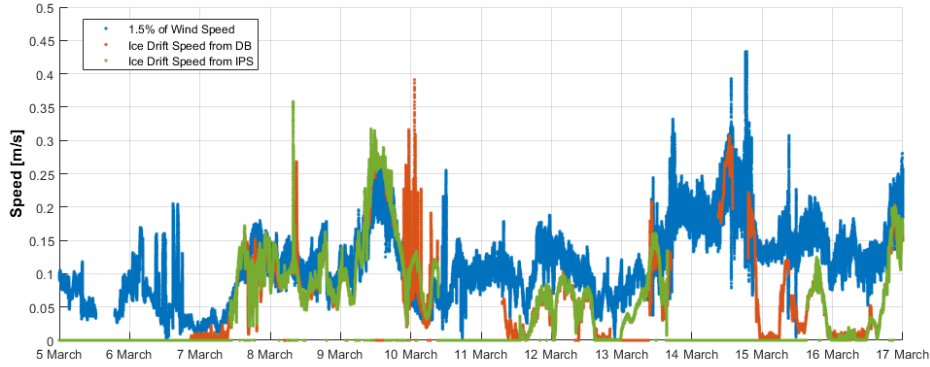
Figure 8. Relationship between the wind speed and ice drift speed during the full-scale measurements

(a)

(b)

(c)
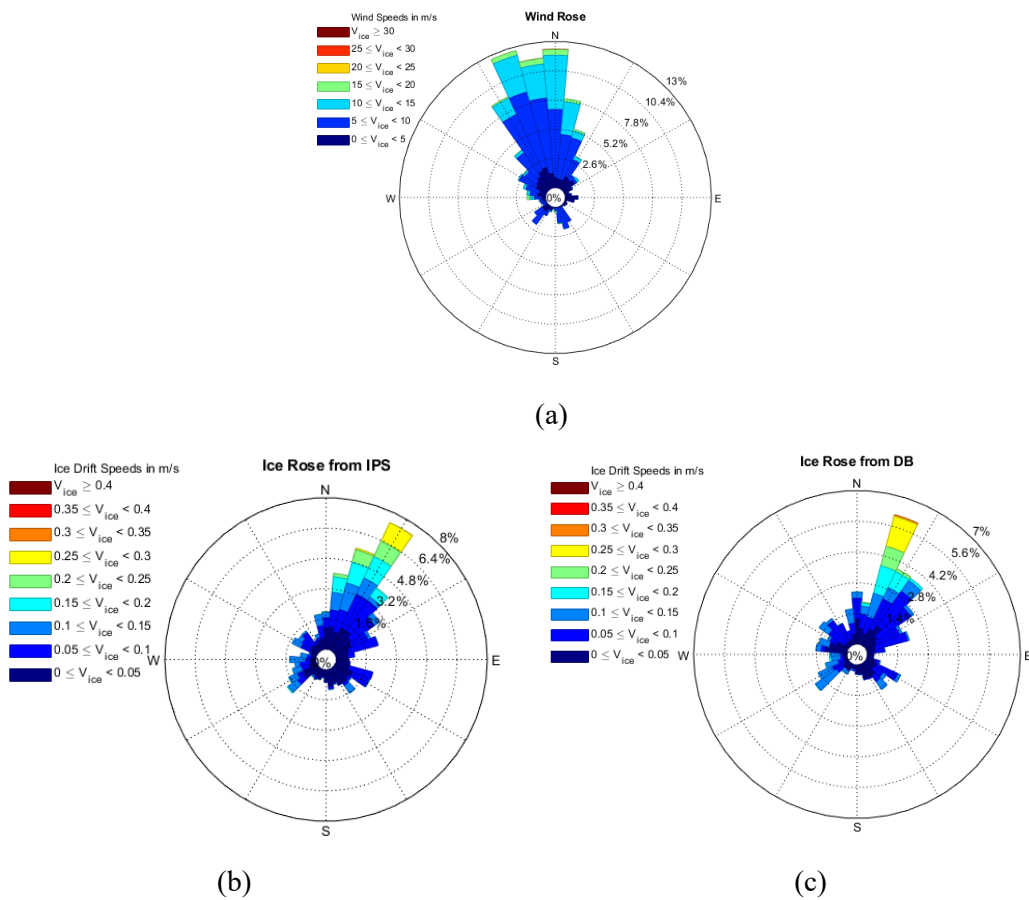
Figure 9. a) the wind rose diagram, b) the ice rose diagram based on IPA, c) the ice rose diagram based on DB
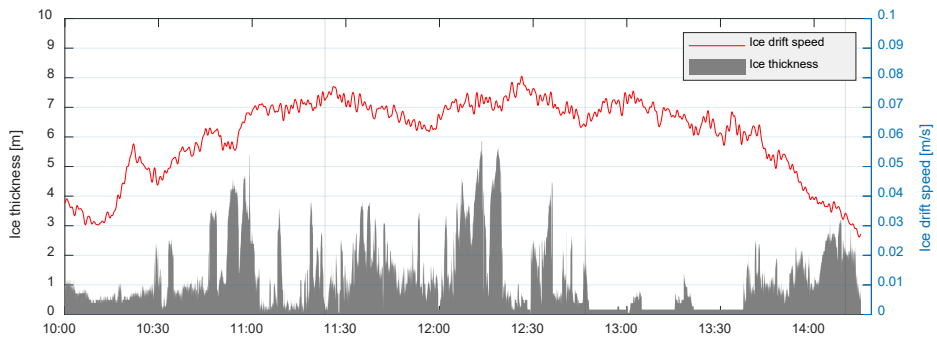
The ice drift speed and ice thickness during the experiment were measured by ADCP and ULS instruments as illustrated in figure 10. The drift speed of the sea ice is highest during case 1: the square updrift pattern. The drift speed is lowest for case 2: the round circular pattern. Sea ice conditions fluctuated the most for case 4: the linear updrift pattern. The mean values of the ice drift speed for each case were listed in Table 4. The sudden drop in the time series of the ice drift speed can be caused either by a complete stop of the sea ice or by loss of the signal from the ADCP measurement.
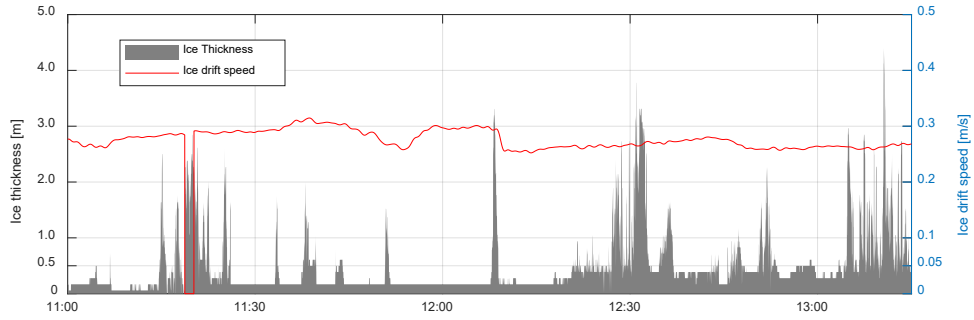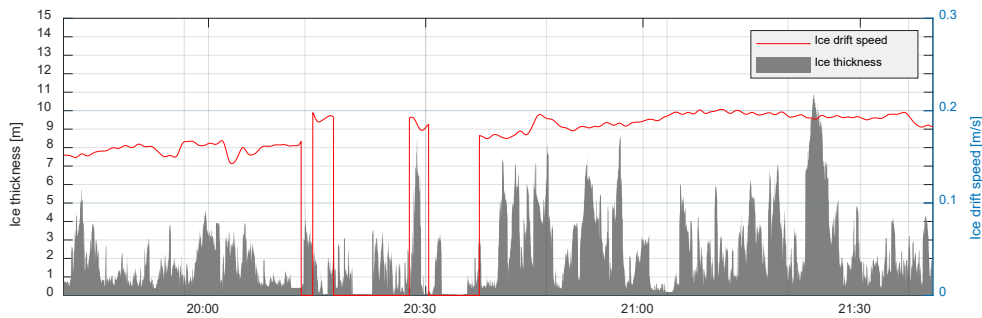
1

2   a)   Ice thickness and ice drift speed during the square updrift pattern
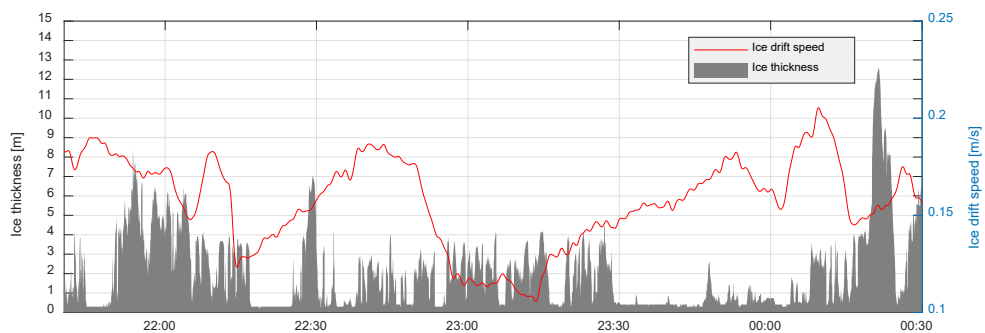

3

4   b)   Ice thickness and ice drift speed during the round circular pattern

5

6   c)   Ice thickness and ice drift speed during the circular updrift pattern

7

8   d)   Ice thickness and ice drift speed during the linear updrift pattern

9

10   Figure 10. Ice thickness and ice drift speed during the full-scale measurements

Table 4 - Statistical characteristics for the ice thickness and ice drift speed

Case	Level ice thickness [m]		Ice draft [m]		Ice drift speed [cm/s]	
	Mean	STD	Mean	STD	Mean	STD
1	0.30	0.16	1.65	0.69	27.32	3.34
2	0.40	0.22	2.00	1.12	6.09	1.31
3	0.52	0.17	2.94	1.92	15.96	5.82
4	0.44	0.14	3.13	1.98	15.74	2.28

Furthermore, the cameras were also deployed in order to record the ice surface around the supply vessel during the experiment. Fifteen cameras were installed and images were recorded once a second. The visual images can be used to estimate the average size of the ice floes as well as the ice drift velocity around the supply vessel (Serre et al., 2018). Moreover, the pictures serve to visualize the characteristics of the surrounding environments such as surface snow cover (if there was sufficient light for the cameras to work). However, due to wind, snow might stick to the camera lenses, which can cause the picture to be more or less blurred. Some illustrations of the ice surface image in front of the supply vessel in the direction of the incoming ice drift for each of the four different test periods are provided by figure 11.
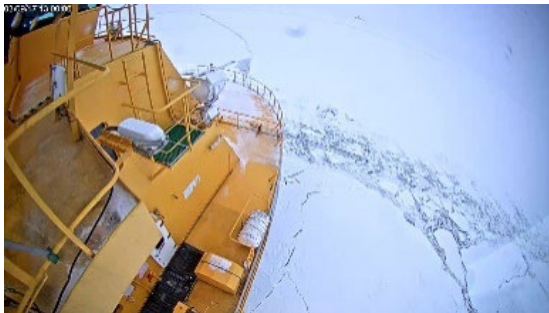
a) 9/03/2017, 13:00:00

b) 12/03/2017, 13:00:00

c) 16/03/2017, 20:00:00

d) 16/03/2017, 23:59:59
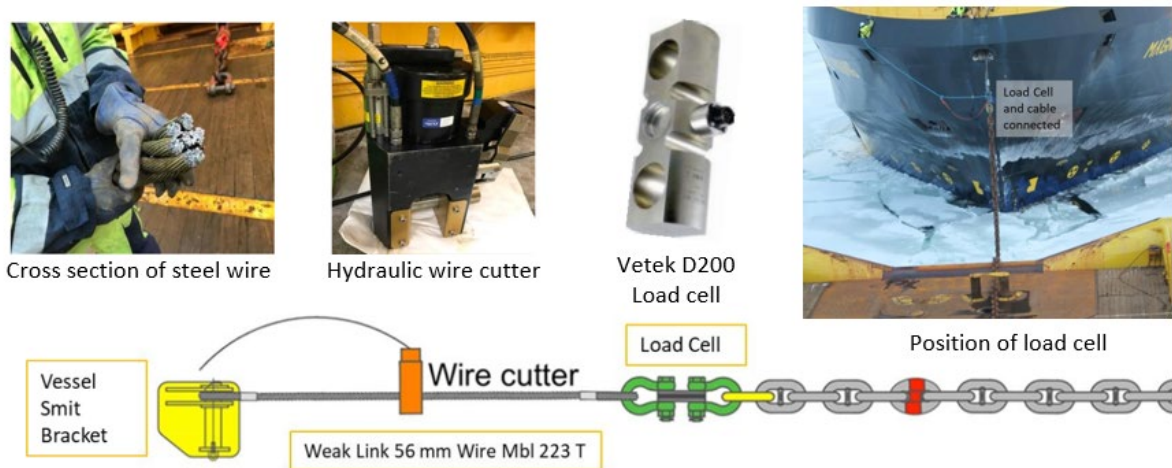
Figure 11. Camera images at MV during the full-scale test

1   2.4 Mooring system

2   The tension in the mooring line during the full-scale experiment was measured by means of a
3   load cell. This instrument was located between the bow of supply vessel, MV, and the mooring
4   chain as illustrated in figure 12. A Vetek D200 load cell was employed to monitor the tension
5   in the mooring line by means of a hard-wired strain-gage with a safe working load (SWL) of
6   150 tons (±0.1%) (Nyseth et al., 2018). The mooring equipment was rented from ISO
7   Intermoor, and the details of the mooring and anchor system are given in Kjøl et al. (2018).

8   The steel wire segment of mooring system has a minimum breaking load of 223 Tons. It is
9   intended as a weak link/ultimate load barrier and will break if the loads exceed the operational
10 limit in the case of an uncontrollable situation. In case of emergency disconnection of the
11 mooring line, a hydraulic wire cutter is installed in the weak link section close to the mooring
12 line attachment point at the forecastle deck of the supply vessel, MV, as illustrated in figure
13 12.

Cross section of steel wire   Hydraulic wire cutter   Vetek D200 Load cell   Position of load cell

Vessel Smit Bracket   Wire cutter   Load Cell

Weak Link 56 mm Wire Mbl 223 T

14

15 Figure 12. Mooring connection arrangement on the supply vessel MV, including wire cutter and
16 loadcell positions (Kjøl et al., 2018)

17

## 3. Theoretical background

3.1 Loading mechanism

The time variation of the tension in the mooring line is obviously dependent on the corresponding time variation of the ship-ice interaction process. Estimation of the resulting total ice-induced loads on the vessel due to drifting sea ice during station-keeping can be obtained by application of the resistance method. Typically, the ice resistance method (Riska, 1997) can be employed to describe the global ice loads of the ice-ship interaction process as well as to estimate the thrust force during for ships advancing in sea ice[6]. For stationary vessels, the ice drift speed can be applied instead of the relative ship speed in order to estimate the global mooring loads. The resistance method is based on summation of loads due to two different mechanisms (Riska, 2011), i.e. the level ice resistance process and the ridge resistance process, respectively, as illustrated in Figure 13.
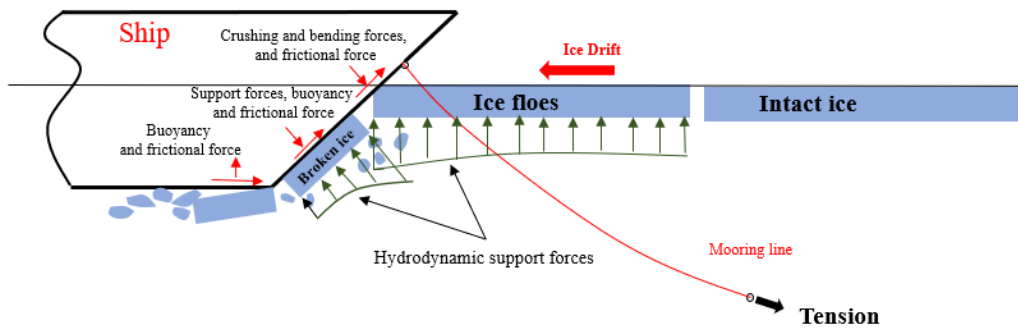
a) The mechanism of level ice and ship interaction
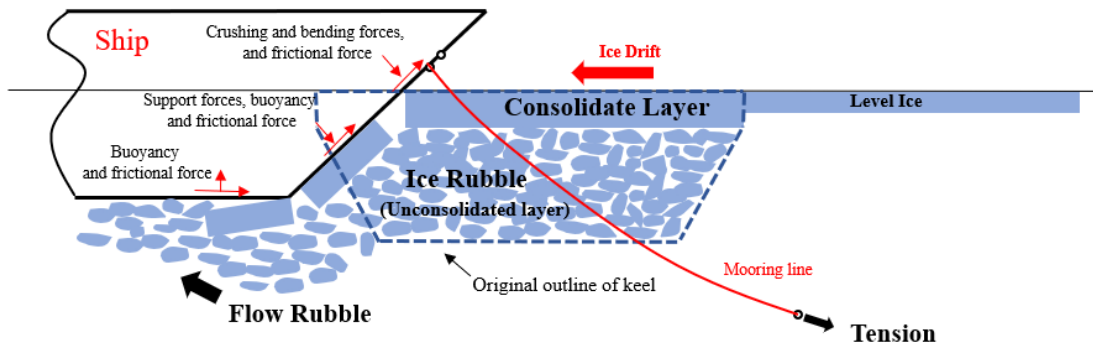
b) The mechanism of ice ridge and ship interaction

Figure 13: The mechanisms of ice and ship interaction processes

The resulting total ice load on the vessel is composed of the level ice component at the bow, $F_i(t)$, the ridge component at the bow (Kuuliala et al., 2017), $F_b(t)$, and ice load acting on middle part of the ship due to the ridge rubble, $F_m(t)$, as expressed by equation 1. Presently, the hydrodynamic loading is not taken into account, since it is assumed to be small compared to the ice loading during the station-keeping experiment.

$$F_{ice}(t) = F_i(t) + F_b(t) + F_m(t) \tag{1}$$

where $F_i(t)$ is the resistance component due to breaking of the level ice, which can be calculated using the ice resistance method by Riska (1997), who derived a simplified expression based on three other basic formulations: Kämäräinen (1993), Ionov (1988) and Lindquist (1989). The expression by Riska (1997) was calibrated using full-scale data from ten Finish merchant vessels with Baltic ice-classes (operating within the same region where the experiments were conducted). The level ice resistance is assumed to a linear function of the ship speed as expressed by equation 2.

$$F_i(t) = C_1(t) + C_2(t) \cdot v(t) \tag{2}$$

where the speed-dependent coefficient C_1 and the speed-independent coefficient, C_2 are expressed by equation 3 and 4. The values of the coefficients that are found on the right-hand side of these two equations are listed in table 5.

$$C_1 = f_1 \cdot \left(\frac{2T}{B} + 1 \right) \cdot B \cdot L_m h_i(t) + (1 + 0.021\phi) \times \left(f_2 \cdot B \cdot h_i(t)^2 + f_3 \cdot L_b \cdot h_i(t)^2 + f_4 \cdot B \cdot L_b \cdot h_i(t) \right) \tag{3}$$

$$C_2 = (1 + 0.063 \cdot \phi) \times \left(g_1 \cdot h_i(t)^{1.5} + g_2 \cdot B \cdot h_i(t) \right) + g_3 \cdot \left(1 + \frac{1.2 \cdot T}{B} \right) \cdot \frac{B^2}{\sqrt{L}} \tag{4}$$

where h_i, B, L, L_b, L_m, ϕ are the level ice thickness, ship breadth at waterline, ship length of waterline, ship length of bow entrance, ship length of parallel midship, stem angle, respectively.

Table 5 - Coefficients entering the level ice resistance formula (Riska, 1997)

coefficients	Value
f_1	230 N/m^3
f_2	4580 N/m^3
f_3	1470 N/m^3
f_4	290 N/m^3
g_1	1890 N/(m$^{2.5}$/s)
g_2	670 N/(m^3/s)
g_3	1550 N/(m$^{3.5}$/s)

The ridge resistance component is calculated by the method presented by Mellor (1980), and it is derived by using Rankine's plasticity model for the ridge rubble. It is assumed to be a cohesionless continuum material. The internal friction angle, ϕ_r is used to characterize the plasticity behavior of the material. The resistance component due to displacing the ridge keel at the bow section can be expressed by equation 5.

$$F_b = C_p \cdot h_r(t) \cdot \left(0.5B + h_r(t)\tan\psi\cos\alpha\right) \times \left(\mu_i\cos\alpha + \sin\psi\sin\alpha\right) \tag{5}$$

where h_r is the local ridge thickness and C_p is a constant that depends on the internal friction angle of the ridge rubble as given in equation 6.

$$C_p = (1-p)\rho_\Delta \cdot g \frac{1+\sin\phi_r}{1-\sin\phi_r} \tag{6}$$

ρ_Δ is the difference between the density of sea water and ice. p is the porosity of the ridge, which varies between 0.25-0.4, and the internal friction angle varies between 47-58 degrees. The density of sea water ice is in the range 890-930 kg/m3 and the density of sea water is about 1025 kg.m^3 (Mellor, 1980).

The midship resistance component, F_m can be expressed by equation 7 (Kuuliala et al., 2017).

$$F_m = C_m \cdot T \int_{L_m} \left(h_r(x) + \left(\frac{h_r(x)}{T} - 0.5\right) \cdot B \right) dx \tag{7}$$

The integration is performed over the parallel midship area from the bow shoulder to the stern shoulder (i.e. L_m) and the term $(h_r(x)/T - 0.5)\cdot B$ is included only when $h_r(x) > 0.5T\cdot C_m$ where C_m is a constant dependent on the Poisson's ratio, v for the ridge rubble given by

$$C_m = \mu_i \cdot (1-p)\rho_\square g \frac{v}{1-v} \tag{8}$$

μ_i is the friction coefficient between ship and ice. g is the acceleration of gravity. The Poisson's ratio, v can have values between 0.21-0.3. The limit depth of ridge keels for the Baltic can be estimated by Hopkins et al. (1991), which is given in equation 9.

$$\lim h_r = 17.64\sqrt{h_i} \tag{9}$$

3.2 Peaks detection of Measured load

The time series of the measured ice induced mooring loads typically consists of a sequence of impulses with quite sharp peaks. The ice-induced loading process has three distinct stages, i.e. the approaching stage, the crushing stage and the disengagement stage. During the full-scale experiments, the ice concentration was very high, i.e. at a level of approximately 9.5 out of 10. For the event with the highest ice concentration, the approaching stage of the ice-induced mooring load is of very short duration as illustrated in figure 14a. The three-stage process of the mooring load is continuously repeated as the ship hull encounters successive ice edges.
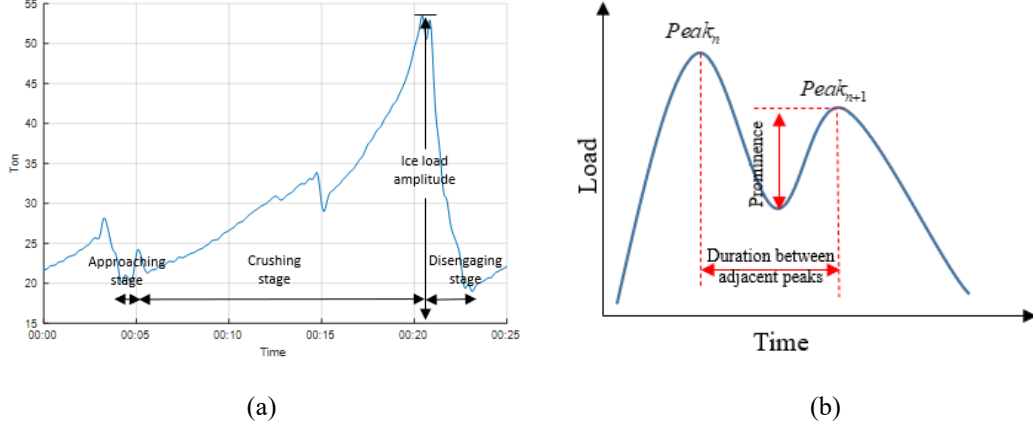
(a)   (b)

Figure 14. a) The three stages of the ice load generation process, b) Concept of the process for peaks prominence detection.

The peaks of the mooring line tension are determined by means of the peaks prominence method implemented in a Matlab toolbox. The procedure behind the peaks prominence method is based on the shortest vertical distance from the lowest neighboring valley to each peaks. The peaks prominence method can be applied in order to avoid that small peaks caused by signal noise are included as part of the recorded time series. An example of a sequence of peaks detections by means of this method is illustrated in figure 14b. The peaks amplitudes of the mooring load are next employed in order to estimate extreme value distributions and to perform the fatigue analysis.

3.3 Extreme value prediction

The extreme mooring loads for each ice management scheme are estimated based on the full-scale measurements. The peaks mooring loads, which were observed at the *MV,* were treated as random variables in order to perform the analysis. The sample values of tension peaks loads, i.e. $t_1,...,t_N$, are assumed to be independent realizations with the same underlying probability distribution, $F(t)$, which is employed in order to establish the extreme value distribution. The probability distribution for the largest value of the mooring load, η , corresponding to a sample of size N is expressed in Equation 10.

$$P(\eta) = \text{Prob}(t_1 \leq \eta,...,t_N \leq \eta) \tag{10}$$

Based on the assumption of independence and identically distributed sample values, Equation 10 can be simplified as expressed by Equation 11:

$$P(\eta) = \prod_{i=1}^{N} \text{Prob}(t_i \leq \eta) = \left[F_t(\eta) \right]^N \tag{11}$$

Here, N is the number of ice load peaks events for the specific period under consideration for each ice management scheme.

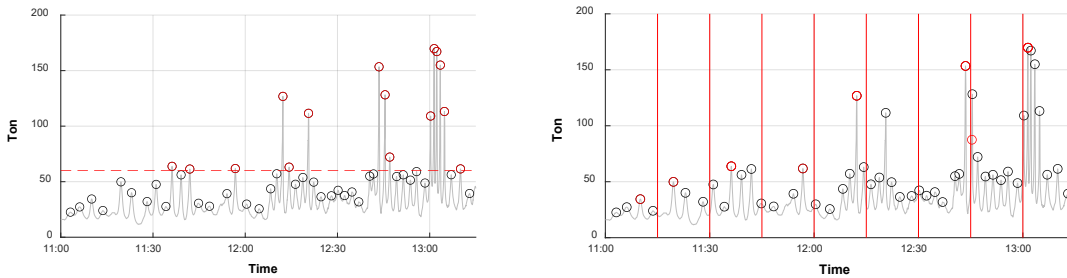3.3.1 The peaks-over-threshold and the block maxima methods

In the present study, two classical approaches for prediction of the extreme loads are applied. These are based on the peaks-over-threshold (POT) and the block maxima (BM) methods. The POT method used here, was first introduced by (Goda, 1989). The load peaks for the mooring lines which have values above a chosen threshold level are applied in order to fit the initial distribution, $F(t)$. The non-exceedance probability $\bar{F}(n)$ based on the no-bias condition (Far and Wahab, 2016) which corresponds to n peaks out of a total number N_{Total} is then given by equation 12.

$$\bar{F}(n) = 1 - \frac{n - 0.44}{N_{Total} + 0.12} \quad \text{for} \quad n = 1,2,3,\ldots, N_{Total} \tag{12}$$

For the BM approach, the values of the peaks mooring loads (within a time window of a fixed duration) are fitted by an initial distribution model that is found to be suitable. Subsequently, this fitted distribution is inserted into equation 11 in order to estimate the extreme value distribution. The extreme value which corresponds to a given exceedance probability, λ, is then obtained from Equation 13.

$$\eta = F^{-1}\left[(1-\lambda)^{1/N_{Box}}\right] \tag{13}$$

Here, the exceedance probability level λ corresponds to a given return period as expressed by equation 14. Furthermore, N_{Box} is the number of blocks into which the measurement record is divided. The relevant peaks values that are applied by the POT versus the BM approach are illustrated in figure 15.

a) Peaks-over-threshold method   b) Block maxima method

Figure15. Illustration of the POT and the BM methods.

For prediction of the short-term extreme mooring load corresponding to the duration of the full-scale experiment, the exceedance probability, λ, (which corresponds to a certain number of repetitions of the operation) can be determined from the return period according to the total number of days being considered, T_{day} (e.g. number of days in one year), as follows:

$$\lambda = \frac{1}{\dfrac{24}{T_{test}} \cdot R \cdot T_{day}} \tag{14}$$

where T_{test} is the duration of a given full-scale test. Here, R is a reduction factor corresponding to the fraction of the time (relative to T_{day}) that the operation is being performed.

For estimation of extreme values, the Gumbel distribution is frequently employed as the initial distribution, mostly because it is assumed to be the appropriate asymptotic distribution for the case at hand. Further justification is rarely provided. The cumulative distribution function (CDF) and the probability density function (PDF) of the Gumbel distribution are given by Equations 15 and 16, respectively:

$$F_{Gumbel}(t) = \exp\left\{-\exp\left[-\left(\frac{t-\beta}{\alpha}\right)\right]\right\} \tag{15}$$

$$f_{Gumbel}(t) = \frac{1}{\alpha}\exp\left(\frac{t-\beta}{\alpha}\right) \cdot \exp\left\{-\exp\left[-\left(\frac{t-\beta}{\alpha}\right)\right]\right\} \tag{16}$$

where β and α are the location and scale parameters of the Gumbel distribution. These parameters can be estimated e.g. by means of least square fitting in probability paper, by the method of moments or by the maximum likelihood method. Moreover, the scale parameters of the BM method compare to the scale parameters of the POT method as expressed in equation 17.

$$\beta_{POT} = \beta_{BM} + \ln\left(N_{Box}\right) \square \alpha_{BM} \tag{17}$$

3.3.2 The ACER method

The average conditional exceedance rate (ACER) method is a numerical approach, which can be applied to investigate the extreme mooring loads for different ice management schemes. The great advantage of using the ACER method is that it provides a unique diagnostic tool for verifying the extreme value distribution inherent in the sampled data. It will produce a nonparametric representation of this distribution, which makes it possible to assess to what extent the asymptotic distributions typically used for the analysis of the extreme value data extracted from the sampled time series actually apply to the case at hand. A central element in the ACER method is the sequence of ACER functions (Naess and Gaidai, 2009) of different order k, converging to the extreme value distribution inherent in the data with increasing k. It can be adopted to analyze the time series realizations of a stochastic process for both stationary and non-stationary data sets. A more detailed exposition of the principles and developments of extreme value estimation with the ACER method is given by Naess and Gaidai (2009) and Naess et al. (2013). The resources needed for using the ACER method for analysis of recorded data, can be found as given in ref. ACER (2013). The formulation of the target probability distribution for extreme value analysis by the ACER method is expressed in equation 18.

$$P(\eta) \approx \exp\left(-(N-k+1)\right) \cdot \text{ACER}_k(\eta) = \exp\left(-(N-k+1) \cdot \hat{\varepsilon}_k(\eta)\right), \tag{18}$$

where, $\hat{\varepsilon}_k(\eta)$ denotes the empirical ACER function of order k, estimated from the data and N denotes the total amount of data of the sampled time series. In principle, increasing accuracy is obtained for increasing order k of the ACER function. However, the k value needed for accurate estimation depends very much on the dependence structure of the time series. With independent data, $k = 1$. For dependent data, a fairly good engineering approximation is obtained for $k = 2$, which corresponds to the classical Poisson assumption of independent upcrossings of high response levels. For extrapolation purposes for data of the kind studied in this paper, the ACER functions are approximated by the following class of parametric functions:

$$\varepsilon_k(\eta) \approx q_k \cdot \exp\left\{-a_k \cdot \left(\eta - b_k\right)^{c_k}\right\}, \quad \eta \geq \eta_0 \tag{19}$$

where a_k, b_k, c_k and q_k are constant coefficients, that are dependent on the order k, and η_0 denotes a tail marker beyond which the approximation in equation 19 is assumed to be valid. The range of values for the ACER coefficients are $a_k > 0$, $b_k \leq \eta_0$ and $c_k > 0$. Note that for this class of parametric functions, the correct asymptotic extreme value distribution is of the Gumbel type, which corresponds to a shape parameter $c_k = 0$. However, when fitting to measured data, which are typically non-asymptotic, the obtained c-parameter would rarely be equal to zero. Hence, in such cases, just assuming the asymptotic Gumbel distribution for the extremes would be highly questionable. In this paper, we shall use the ACER method for the specific purpose of verifying the validity of this assumption for our data.

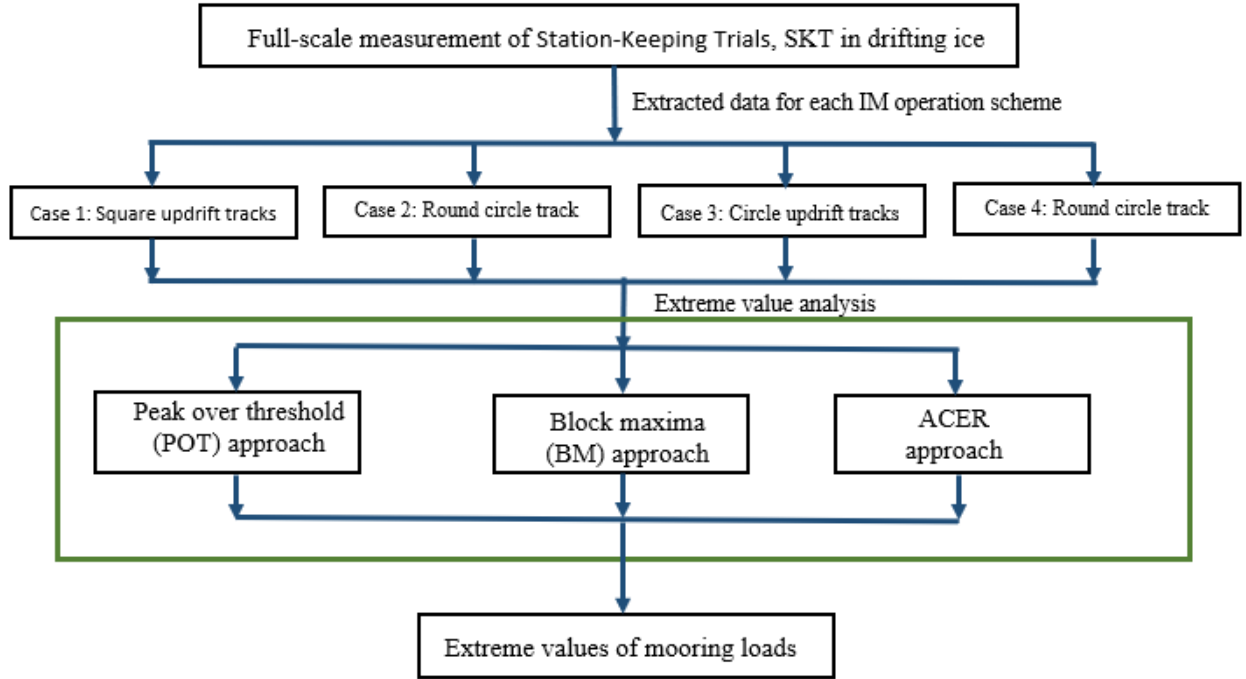The procedure for estimation of the extreme mooring load is illustrated in figure 16.

Figure 16. Flowchart of the steps required for extreme value prediction of mooring loads.

3.4 Fatigue damage evaluation

The accumulated fatigue damage of the mooring line during a particular short-term condition can be estimated by application of the Palmgren-Miner rule as expressed in equation 20.

$$D_{total} = \sum_{i=1}^{w} \frac{n_i}{N_i} \tag{20}$$

where D_{total} denotes the fatigue damage during the short-term condition corresponding to a given ice management scheme; n_i is the number of stress cycles for the specific IM operation scheme; N_i denotes the number of stress cycles to failure of a particular mooring line component corresponding the particular stress range, S_i.

Fatigue strength can be described by the SN curve approach, which was originally introduced by Wöhler (Naess, 1985). The SN curve to applied in order to perform the fatigue assessment is typically formulated as given in equation 21.

$$N_i = A \cdot S_i^{-m} \tag{21}$$

Here, A and m denote the intercept parameter and the slope of the SN curve, respectively. These parameters are related to the category of the mooring line, i.e. stud chain, studless chain (open link), stranded rope, spiral rope, etc. In DNVGL (2015) a single slope SN curve without endurance limit is recommended for mooring lines. The mooring load, t, is measured by means of the load cell. Accordingly, the axial stress, σ_{normal}, in the mooring line can be calculated by dividing with the cross-section area:

22

$$\sigma_{normal} = \frac{t}{Area} \tag{22}$$

In which, $Area = \frac{2\pi d^4}{4}$ for the chain, where d is the diameter of a mooring chain component.

There are several counting methods in order to determine the stress range such as counting of level crossings , peaks counting, sample range counting, rainflow counting etc. (Naess, 1985). In this study, the stress range and the number of stress cycles for the mooring line is estimated by means of the rainflow counting algorithm, which was first proposed by Matsuishi and Endo (1968). An illustration of the rainflow counting algorithm for the recorded Mooring Load during the full-scale experiment is provided by figure 17.
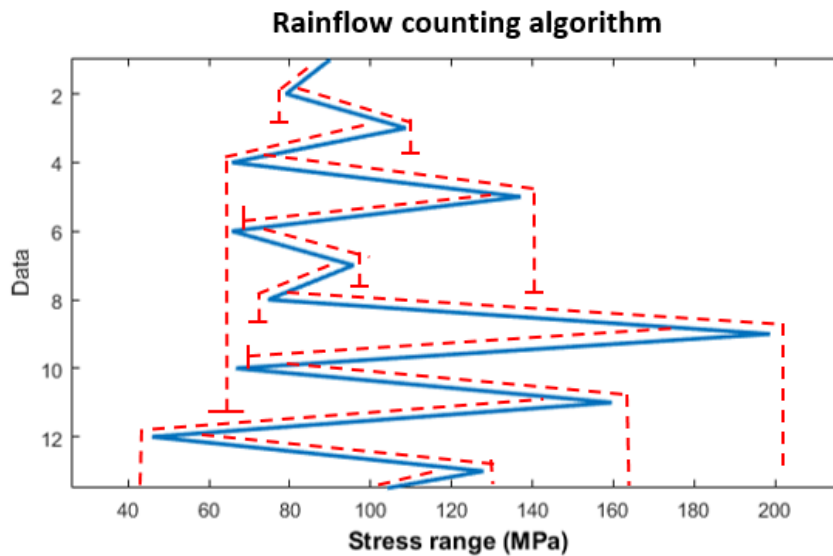
Figure 17. Example of rainflow counting algorithm for determination of stress ranges in the mooring line

The parameters A and m which define the SN curve are given in Table 6, and the corresponding SN curve itself is shown in figure 18.

Table 6: SN-fatigue curve parameters for mooring lines, DNVGL-OS-E301(2015)

Item	Intercept parameter, A	SN curve slope, m
Stud chain	1.2×10^{11}	3.0
Spiral rope	1.7×10^{17}	4.8
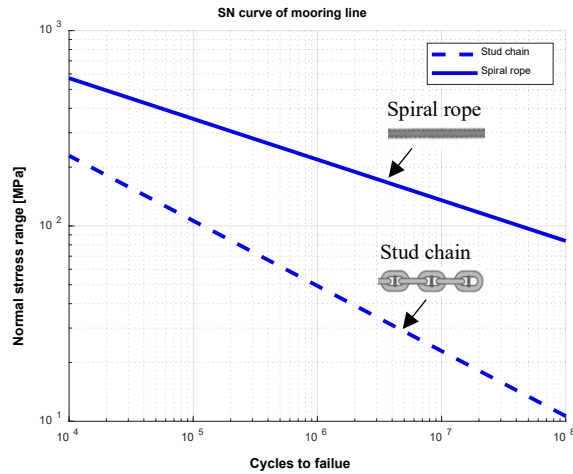
Figure 18. SN curve of mooring lines for stud chain and spiral rope
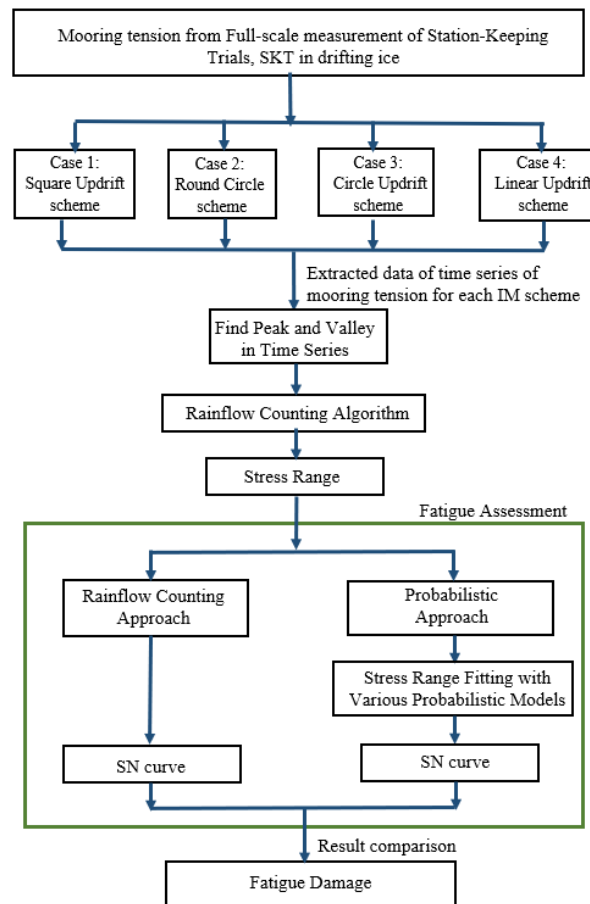
Figure 19. Procedure for probabilistic fatigue assessment of mooring lines

The SN curve in equation 21 can be substituted into equation 20 in order to determine the total fatigue damage. This gives:

$$D = \frac{1}{A}\sum_{i=1}^{w} n_i S_i^{m} \tag{23}$$

For application of the stochastic assessment, the fatigue damage in equation 20 can be written in connection with the probabilistic distribution of the stress range of mooring lines as expressed in equation 24. The probability, $P(n_i)$ of stress number, $n_i(S_i)$ that occurs during the total number, N_T of stress cycles can be written as

$$P(n_i) = \frac{n_i(S_i)}{N_T} \tag{24}$$

On the other hand, the probability that the stress range S_i will occur can be found as the area under the probability density function, and this can be expressed by equation 25.

$$P(S_i) = f_s(S_i) \cdot \Delta S_i \tag{25}$$

Since equations 24 and 25 represent two ways of expressing the same probability, the two expressions can be set equal to each. This equation can be solved with respect to the number of stress cycles corresponding to a given stress range, i.e. $n_i(S_i)$:

$$P(n_i) = P(S_i) \tag{26}$$

$$\frac{n_i(S_i)}{N_T} = f_s(S_i) \cdot \Delta S_i \tag{27}$$

$$n_i(S_i) = N_T \cdot f_s(S_i) \cdot \Delta S_i \tag{28}$$

Equation 28 can be inserted in equation 20 in order to compute the fatigue damage, D, as given in equation 29.

$$D = \sum_{i=1}^{w} \frac{n_i}{N_i} = \frac{N_T}{A}\sum_{i=1}^{w} S_i^{m} \cdot f_s(S_i) \cdot \Delta S_i \tag{29}$$

For continuous values of the stress range, equation 29 can be rewritten in terms of an integral as given in equation 30:

$$D = \int_{0}^{\infty} \frac{N_T}{A} \cdot S^{m} \cdot f_s(S)\,ds \tag{30}$$

where $f_s(S)$ is the probability distribution of the stress ranges, which can e.g. be obtained by application of the Rainflow counting algorithm. The probability distribution of the stress ranges can also be described e.g. by the Weibull distribution, the lognormal distribution or the exponential distribution. The corresponding expressions for the probability density functions are given by equation 31 to equation 33, respectively.

$$f_{Weibull}(S) = \frac{h}{q}\left(\frac{S}{q}\right)^{h-1} \exp\left(-\left(\frac{S}{q}\right)^{h}\right) \tag{31}$$

where, h and q are the shape parameter and scale parameters of the Weibull distribution,

$$f_{Lognormal}(S) = \frac{1}{\sigma s\sqrt{2\pi}} \exp\left(-\frac{(\ln(S)-\mu)^2}{2\cdot\sigma}\right) \tag{32}$$

where, μ and σ are the parameters of the log-normal distribution and

$$f_{Exponential}(S) = \lambda\cdot\exp(-\lambda\cdot S) \tag{33}$$

where, λ is the parameter of the exponential distribution

From equation 30, the upper limit of integration can be specified to be the minimum breaking mooring loads as expressed in equation 34.

$$D = \int_{0}^{S_{MBL}} \frac{N_T}{A}\cdot S^m \cdot f_s(S)ds \tag{34}$$

A flowchart of the fatigue assessment procedure applied in the present study is illustrated in Figure 19

4. Results

For the full-scale experiment of SKT project, the ice breaker, TV is deployed for the purpose of ice management in order to break the sea ice in the updrift direction relative to the stationary supply vessel so as to reduce the ice loads on this vessel. In the experiment, the ice drift behavior was monitored by two types of instruments at the local station by ADCP measurements and an ice drift beacon, which was installed on the sea ice (Teigen et al., 2018). The ice rose diagram (Sinsabvarodom et al., 2019) can be applied to demonstrated the ice drift speed and direction of the sea ice during the IM operations. The traveling tracks of the ice breaker and supply vessel for each pattern scheme during the IM operations characterized by the latitude and longitudinal angles as demonstrated in figure 20. Four different schemes for ice management are implemented. The real tracks of the ice breaker during each IM operation are slightly different from the planned ones because of the variation in ice thickness, ice drift speed and the ice breaking capabilities of the vessel.
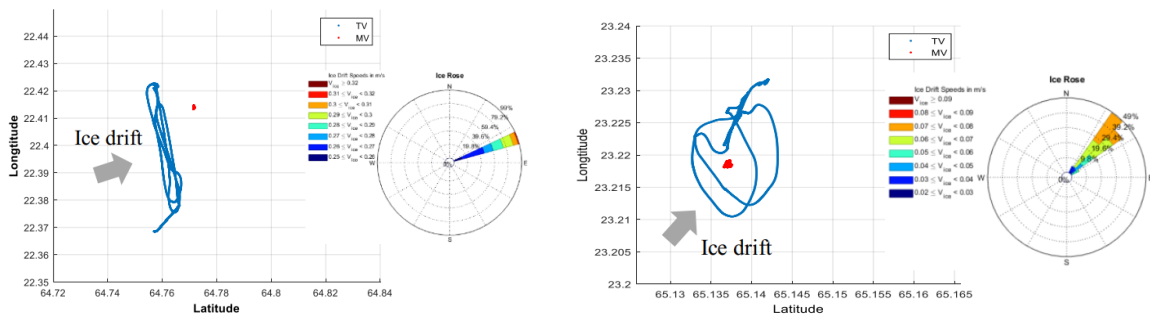
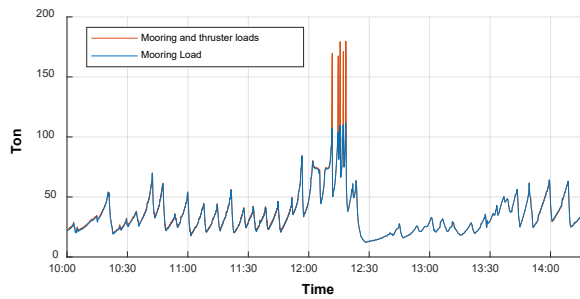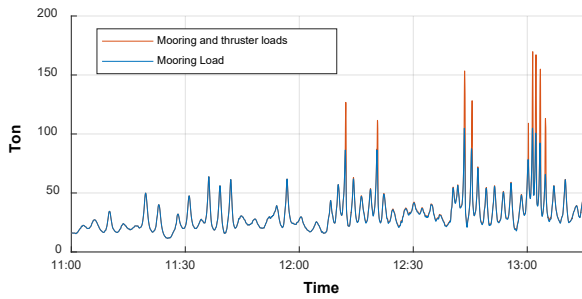**(a) Case 1: Square updrift pattern**   **(b) Case 2: Round circular track**
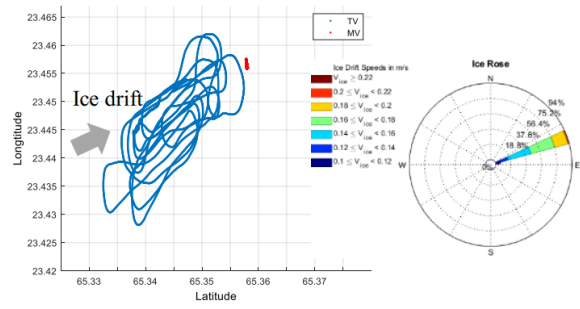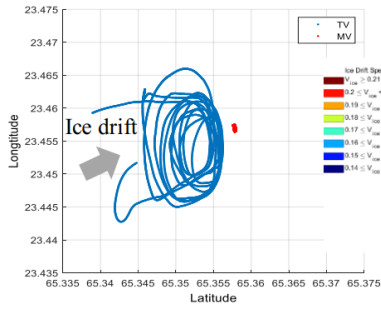
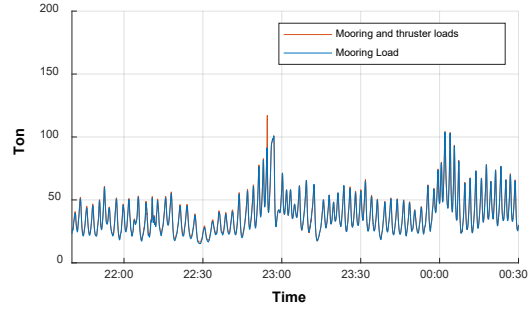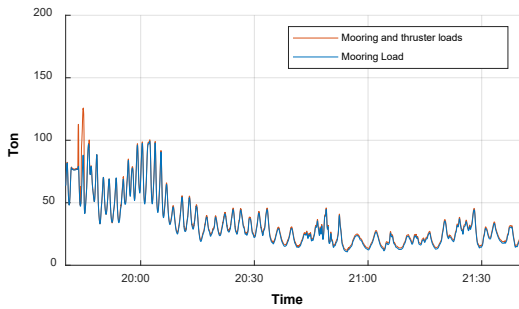**(c) Case 3: Circular updrift tracks**   **(d) Case 4: Linear updrift track**

Figure. 20 Trajectories of TV and MV during the IM operations for station-keeping trials in drifting ice

Time series of mooring tension during each of the IM operations are recorded by means of the load cell with one recording every second. The thrusters of the supply vessel, MV were also activated for the purpose of dynamic positioning assisted mooring (DPAM) when the mooring load reached a level of 100 tons as illustrated in the figure 21.

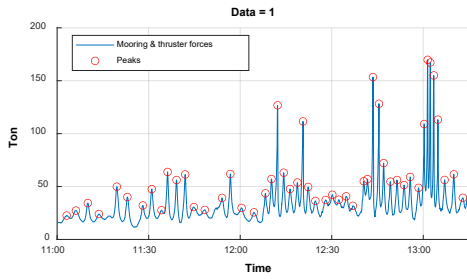**(a) Case 1: Square updrift tracks**   **(b) Case 2: Round circular tracks**

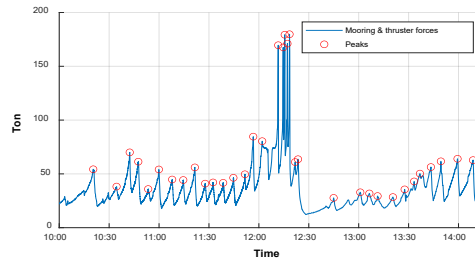**(c) Case 3: Circular updrift tracks**   **(d) Case 4: Linear updrift tracks**

Figure 21. The Mooring and active thruster forces for different ice management schemes

The load peaks in the mooring line and thrusters were computed by using the peaks prominence method in order to avoid the local peaks caused by signal noise. The value of the minimum prominence for peaks detection was set equal to 2 tons in the analysis. The results of the peaks detection for the time series of the mooring load for different cases of IM operations are demonstrated in figure 22.
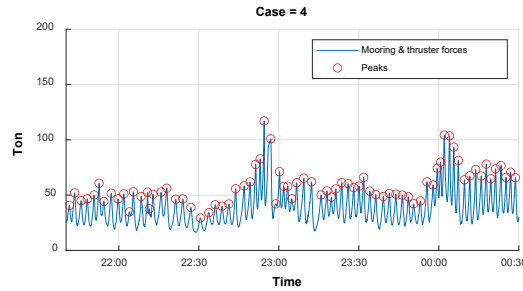
(a) Case 1: Square updrift tracks

(b) Case 2: Round circular tracks
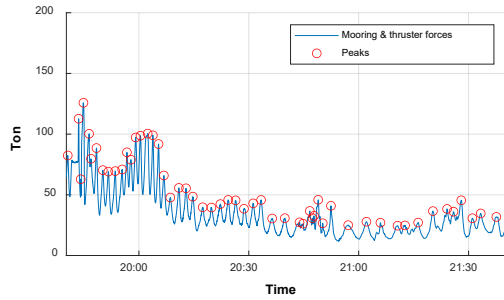
(c) Case 3: Circular updrift tracks

(d) Case 4: Linear updrift tracks

Figure 22. Mooring and thruster forces for different ice management schemes

The example of active thrusters to support the mooring line during the appearance of an ice ridge is as illustrated in figure 23. The weakest link in the mooring line componence is at the load cell which has a maximum capacity of around 150 tons. In the present study, the total loads from mooring line and thruster are employed for the purpose of short-term extreme mooring load analysis.
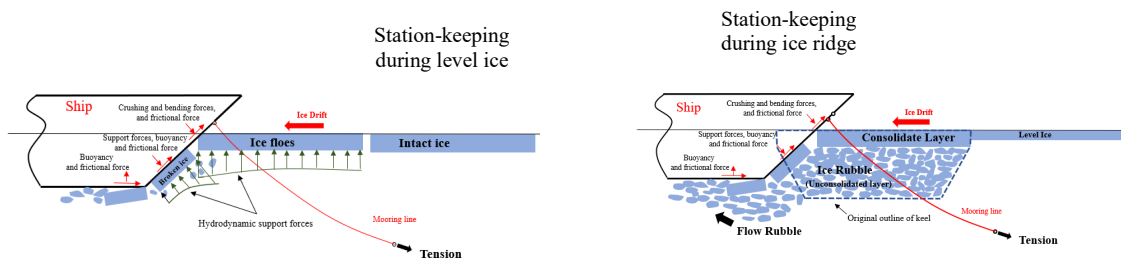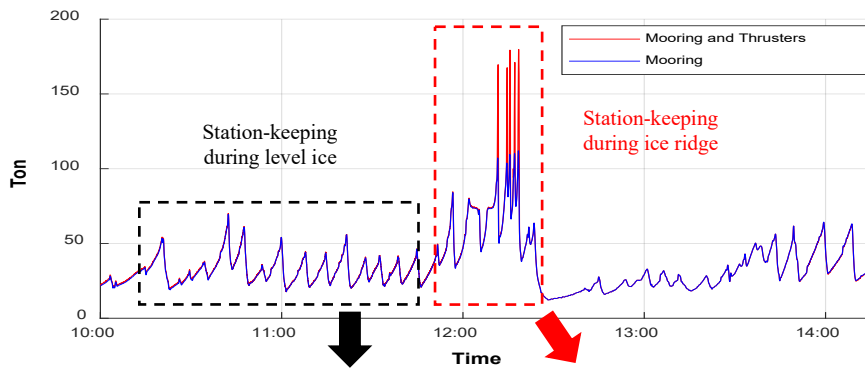

Figure 23: The example of active thrusters to support the mooring line for case 2: Round circular tracks.

4.1 Estimation of global ice loading

The global ice loads on the vessel are calculated by means of the ice resistance method by application of the measured time series of the ice thickness and ice drift speed and these loads are compared with the recorded mooring loads during ice management. Since the ice resistance method does not take into account the effect of the ice management, this will give rise to a systematic difference as seen from the two sets of histograms in Figure 24. Fenz et al. (2018) also found from the full-scale experiment obtained during the OATRC 2017 project that the local ice pressure on the ship bow is substantially reduced for well organized ice management operations. A comparison between the statistical parameters of the measured versus the calculated ice load are listed in table 7. Note that for the calculated loads, the differences between the results for the different cases are solely due to the variation in the ice thickness and the drift speed (and not take into account the differences in the ice management schemes). The statistical variation of the calculated load is estimated based on the statistical characteristics of the input variables (i.e. the ice thickness and drift speed), see e.g. Sinsabvarodom et. al. (2020a).

Table 7: The statistical parameters of the mooring loads for each IM scheme

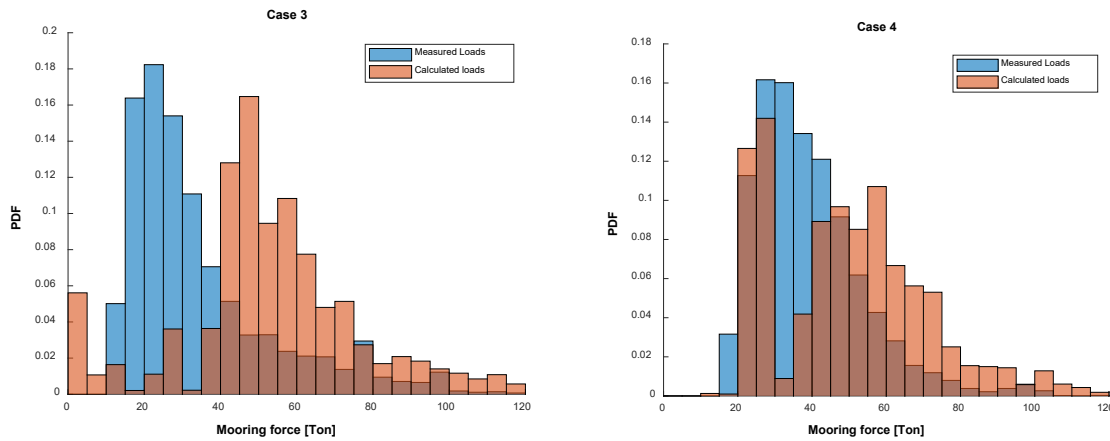| Case	Measured Load [Ton]			Calculated Load [Ton]		
	Mean	STD	COV %	Mean	STD	COV %
1	32.22	17.03	52.85	24.92	16.11	64.63
2	35.08	17.99	51.29	41.63	18.99	45.61
3	34.89	20.15	57.76	55.13	26.88	48.76
4	39.07	14.69	37.60	52.30	27.02	51.67
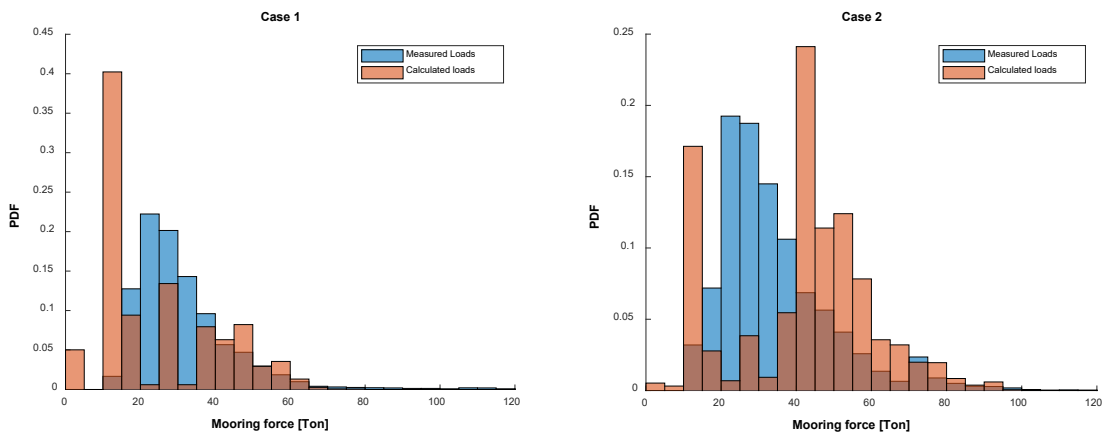
Figure 24: Histograms of data distribution between measured mooring load and calculated (undisturbed) global ice load for each ice management scheme

4.2 Extreme value estimation

Typically, the extreme loading conditions are applied to the design of ships and offshore structures. In the cold regions, sea ice load become the major loading that exert to the structures. Typically, sources of the uncertainty in the ice loading comes from the sea ice properties during the sea ice formation (Sinsabvarodom et al., 2020a). The extreme value theory can be applied to the design key parameter of the ice load, such as ice thickness, ice drift speed etc., in order to predict the extreme ice load that subject to the mooring lines for the structural design. The other way around, the extreme value of mooring load can be directly estimated from the physical measured data of loading time series. In this research, the extreme mooring load is performed based on the measured data of the peak loads in the recorded time series. The ice data and metocean condition during SKT project is given in Teigen et al. (2018).

4.2.1 The peaks-over-threshold and the block maxima methods

The peaks values of the mooring load time series are used to perform the short-term extreme value analysis. The results for extreme mooring loads estimated by the peaks over threshold (POT) method and the block maxima (BM) method are compared. The peaks data points for the BM method are fitted to various probabilistic models in order to determine the initial distribution (or parent distribution) to be applied for the extreme value analysis. Subsequently, the Gumbel distribution is found to provide the most appropriate fitting of the extreme mooring load peaks for both the POT and BM methods. Examples of fitting the peaks mooring loads by the Gumbel distribution for both the POT and BM methods for the case corresponding to the Square updrift pattern are illustrated in figure 25.
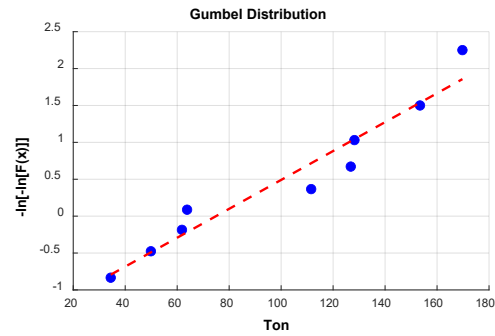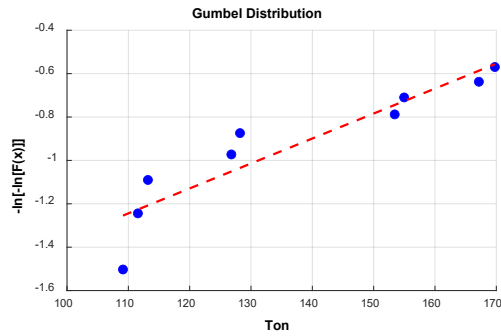
(a)   (b)

Figure 25: a) Example of data fitting by the peaks-over-threshold method, b) Example of data fitting by the block maxima method for the case 1: Square updrift pattern.

Table 8 - The shape and location parameters of the Gumbel distribution based on extreme value analysis by the POT and BM methods

	Reference duration (Hour)	Peaks over threshold (POT)			Block maxima (BM)			
		Threshold (Ton)	Location parameter	Scale parameter	Time window (minutes)	Numb. of block	Location parameter	Scale parameter
Case 1	2:15	80	218.1	86.9	15	9	187.13	51.06
Case 2	4:25	85	197.3	23.1	15	17	171.71	46.85
Case 3	2:00	65	117.2	45.0	10	12	123.17	33.03
Case 4	2:50	68	131.6	53.2	25	7	128.60	30.03

It is found that the extreme mooring load distribution obtained by the POT and the BM methods are sensitive respectively to the applied value of the threshold and to the length of the time window. Examples of extreme mooring load PDFs obtained by varying the threshold value for case 3 are illustrated in figure 26a. The proper threshold value to be applied by the POT method needs careful consideration since higher threshold values will result in a smaller and smaller number of data points to be applied for the fitting.
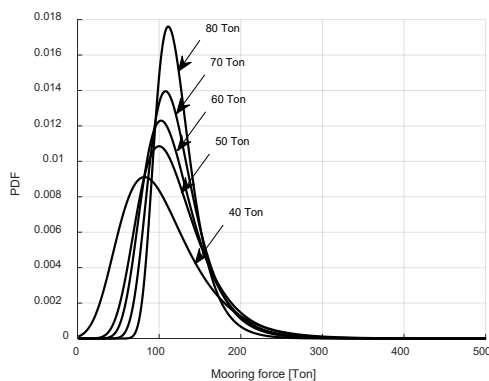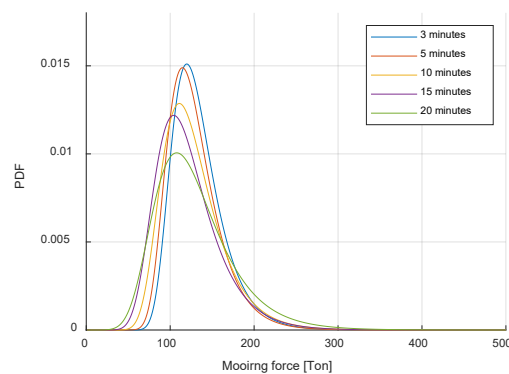

a)   (b)

Figure 26: a) Examples of extreme mooring load PDFs by varying the threshold values for the POT method for the case with circular updrift pattern, b) Example of extreme mooring load PDFs by varying the length of the time windows for the BM method

The time window for extreme mooring analysis is longer than the time window for the extreme ice loads on the ship hull itself, which is typically about 1 to 5 minutes (Chai et al., 2018a; Suyuthi et al., 2012b). This is due to the peaks mooring loads being caused by the integrated effect of all the local ice loads acting on the ship hull. The station-keeping ship has almost zero speed for initial condition of ship-ice interaction process. This causes the interval between the mooring load peaks to be longer than the interval between the local ice load peaks. For the results of the present full-scale experiment, the duration of the time window for the BM method, can be selected within the range from 3 to 20 minutes approximately. The Examples of sensitivity studies with respect to the duration of the time window for the BM method (for case 3: the circular updrift pattern) are illustrated in figure 26b.

The location and shape parameters of the Gumbel extreme value distribution obtained by the POT and BM methods are listed in table 5. The location parameters of the parent distributions applied by the BM method which are given in the table 8 were calculated from equation 17 in order to compare with the location parameters for the POT method.

The PDFs of the extreme peaks loads obtained by the POT method tend to provide higher values than the BM method, but with case 3 being an exception. Suyuthi et al. (2012b) also performed extreme value estimation by using the initial distribution for the load peaks and applying the number of peaks data points to be equal to the parameter N_{Box} in equation 13. This provides extreme load distributions close to those obtained by the BM method. A comparison of extreme mooring load PDFs obtained by the POT and BM methods for each pattern of IM operations is shown in figure 27.
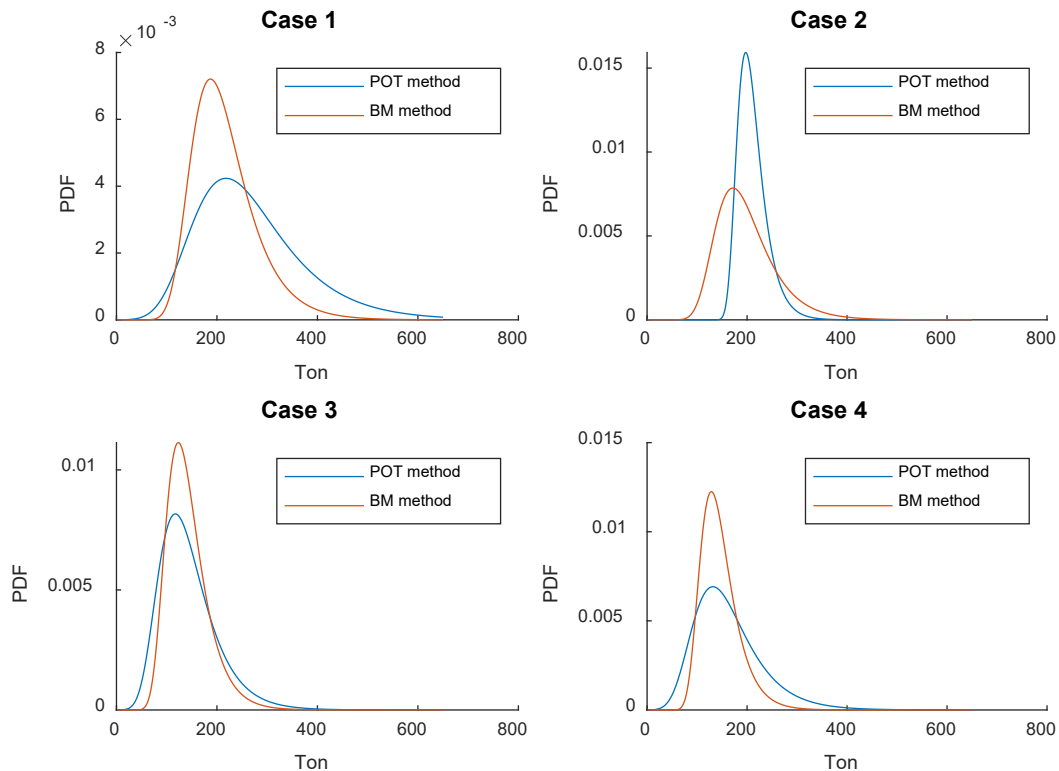

Figure 27: Comparison of extreme mooring load PDFs obtained by the POT and BM methods for each pattern of IM operations

During the full-scale measurements, the mean values and standard deviations of the level ice thickness, the ice draft and the ice drift speed are recorded as shown in figure 28a, 28b and 28c, respectively. The statistical parameters of the level ice thickness and the ice draft/ridges were calculated from the recorded IPS time series. However, the records of ice draft from the IPS is unable to distinguish between level ice thickness, consolidated layer or ice rubble. Therefore, the maximum values of the last ten years from drilling data related to level ice thickness (Ronkainen et al., 2018) in the Bay of Bothnia were used to distinguish between the data pertaining to the level ice thickness and the ice draft/ridges in the time series.

The maximum level ice thickness and the ice draft occurred during the IM operations for case 3 and 4, respectively. The highest ice drift speed occurred for case 1: the square updrift pattern, while the ice thickness and the ice draft had the lowest mean values for this case.

a)

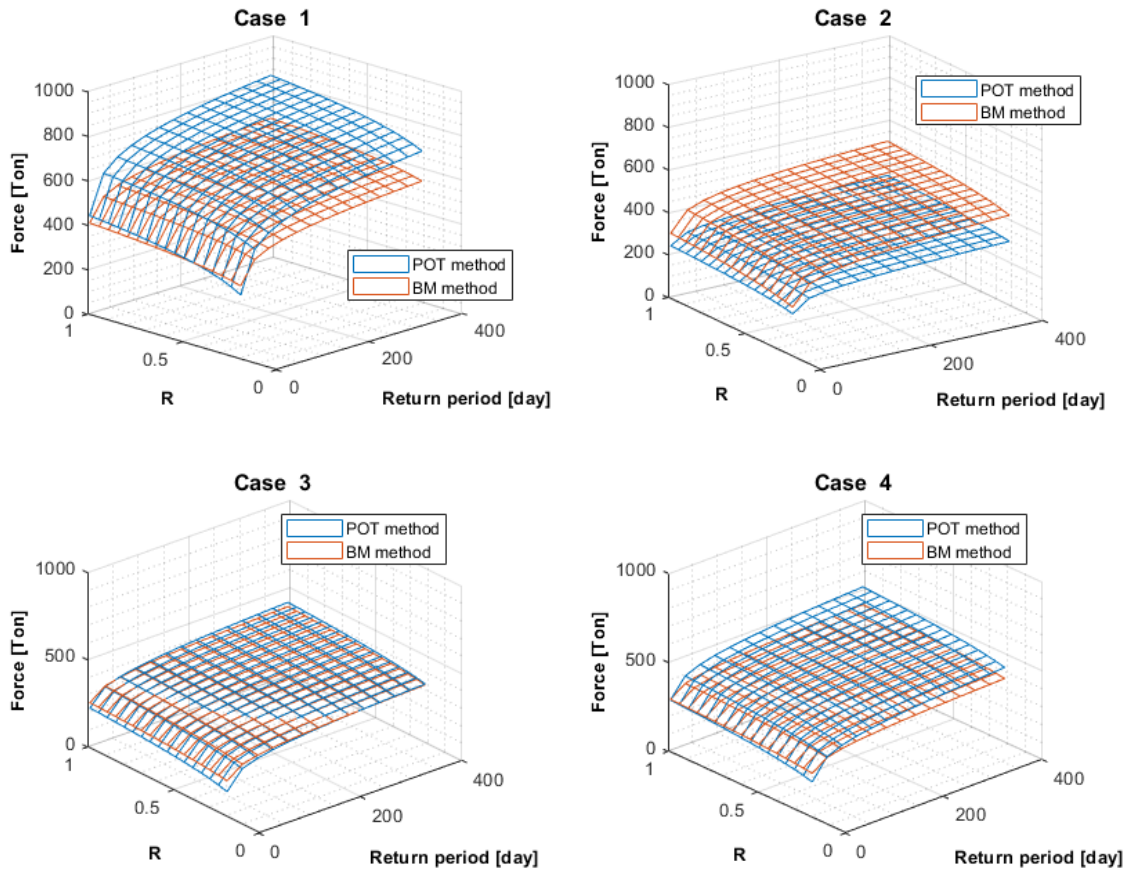(b)

(c)
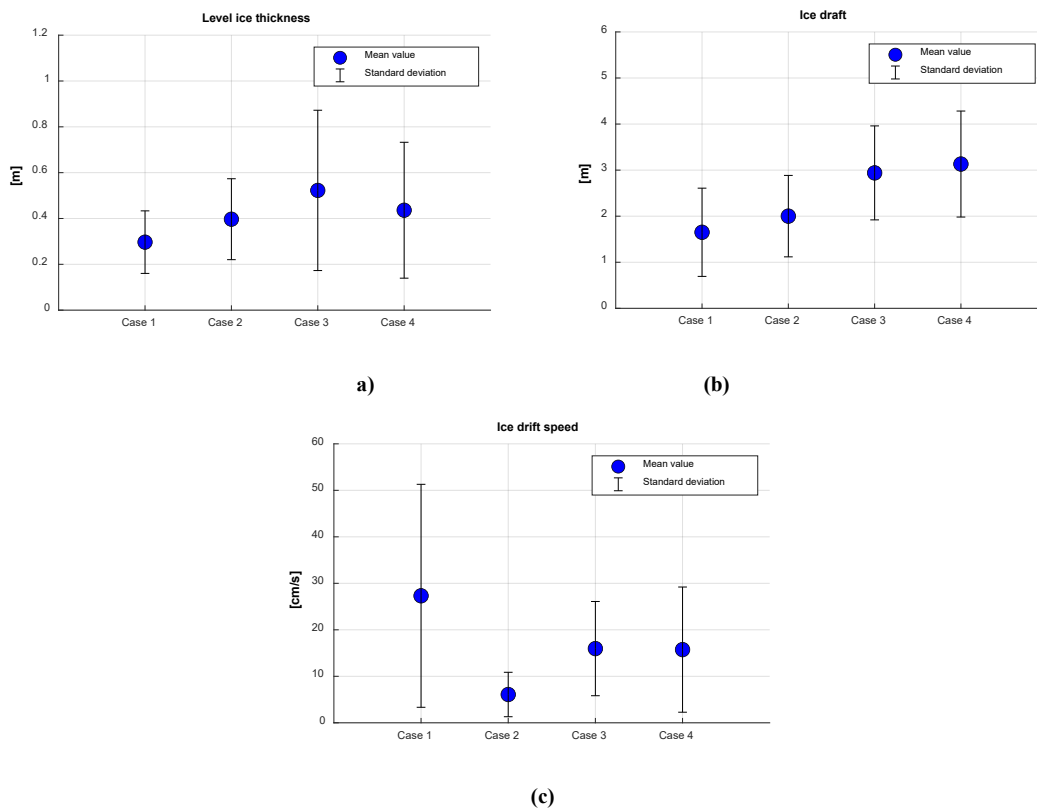
Figure 28. a) The level ice thickness during ice management operations, b) The keel depth of the ice draft/ridge during ice management operations, c) Ice drift speed during ice management operations.

Figure 29. Comparison of extreme mooring force estimated by different methods corresponding to different return periods including the effect of the reduction factor, *R*

The results for the short-term extreme mooring loads obtained by the POT and BM methods exhibit similar trends. Both methods predict an increase of r magnitude for the extrapolated long-term extreme mooring loads corresponding to different return periods, also combined with the reduction factor, *R* according to the equation 14, for each IM operation as illustrated in figure 29. The maximum difference between the long-term extreme mooring loads obtained by the two methods is approximately 25 percent.

4.2.2 The ACER method

For the purpose of verifying the simplistic approaches to extreme value estimation presented in section 4.2.1, the diagnostic power of the ACER approach is now applied to the available sampled data. The recorded time series for each IM scheme are used in full for estimation of the ACER functions by using $k = 2$ in accordance with the discussion on section 3.3.2. The empirical ACER functions, $\hat{\varepsilon}_k(\eta)$, for $k = 2$, are plotted versus the amplitude of mooring loads for each case in figure 30. Note that a Gumbel extreme value distribution would correspond to a straight line in these plots. Taking into account the really meagre amount of data available, the plots of the ACER functions do in fact point to the conclusion that the Gumbel distribution is a fairly good and workable approximation of the extreme value distribution inherent in the data. This provides a reasonably sound basis, even in the face of very limited amounts of data, for its use in the BM method adopted in this paper.
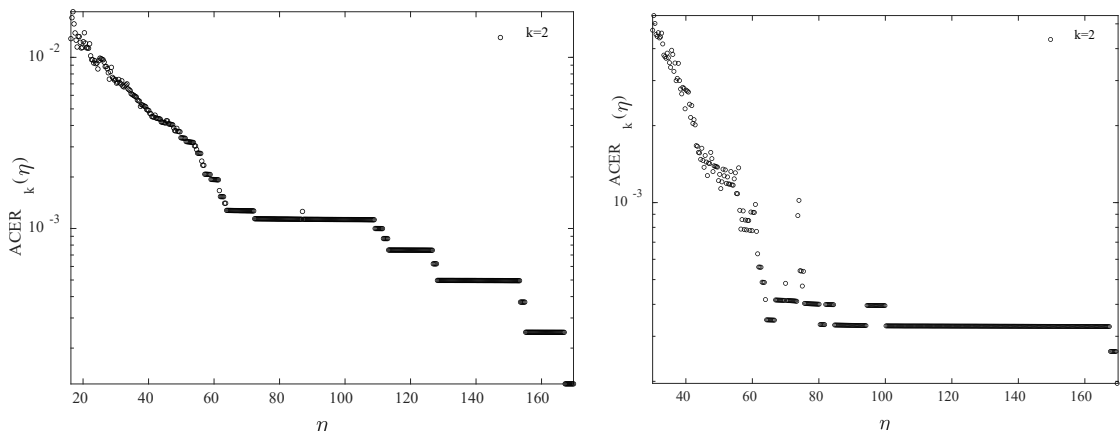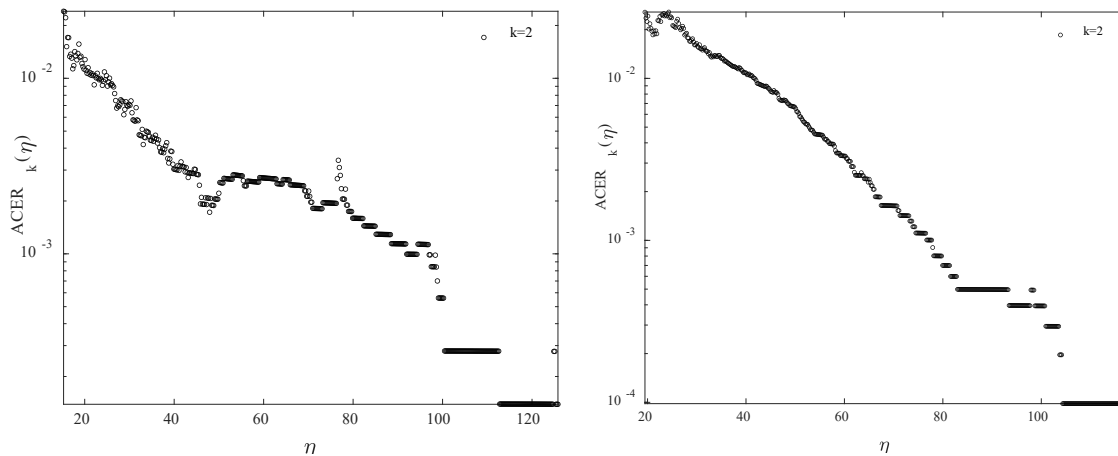

(a) Case 1: Square updrift pattern   **(b) Case 2: Round circle pattern**

(c) Case 3: Circular updrift pattern   **(d) Case 4: Linear updrift pattern**

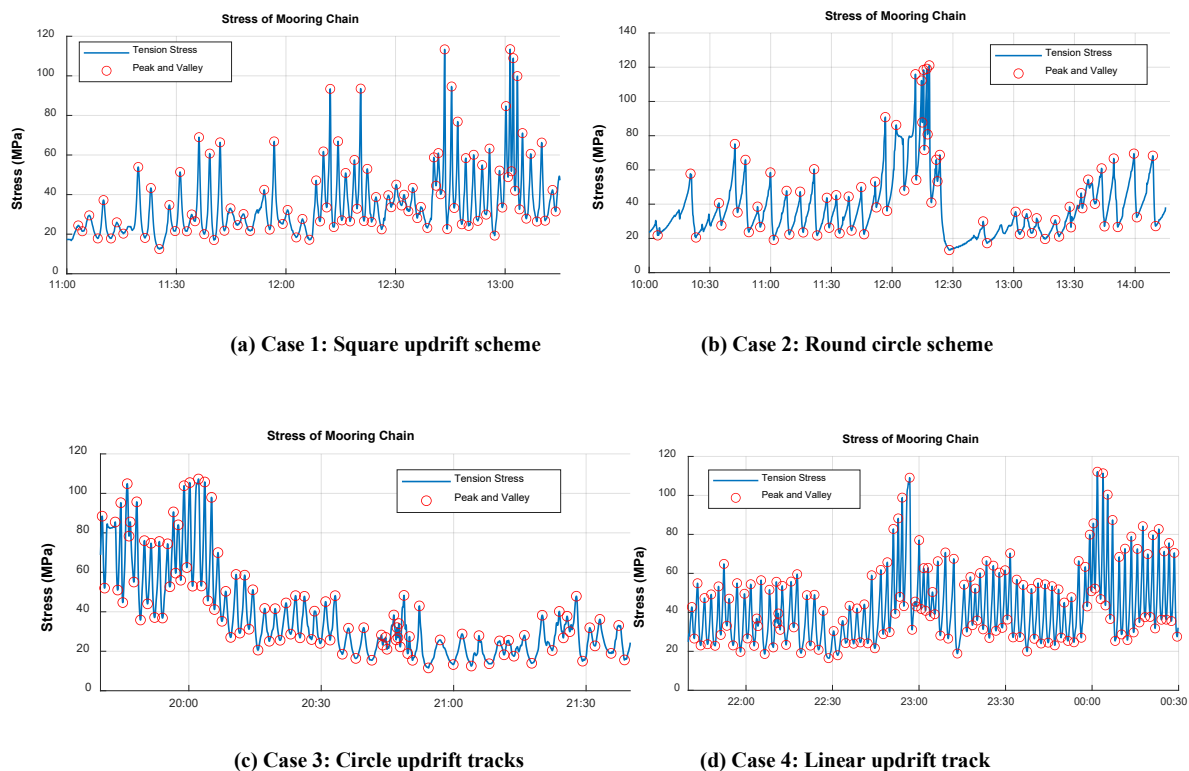**Figure 30.** Plot of barrier levels η versus ACER functions $\varepsilon_k(\eta)$ for k = 2 on the logarithmic scale for different ice management schemes

When the Gumbel distribution is an acceptable approximation for the extreme value distribution, then the ACER method and the BM method would give more or less the same results if properly implemented. However, for cases with little data it is recognized that there is considerable uncertainty associated with the estimates obtained by the different methods. Due to the simplicity of application of the BM method, and having verified its applicability for our data, we use it as a reference method in this paper.

4.3 Fatigue damage based on probabilistic models

The short-term fatigue damage of the mooring line during the full-scale experiments caused by the ice loading on the supply vessel corresponding to each ice management operation is estimated in the following. The fatigue damage accumulation for the steel chain, which is a major component of the mooring system, is calculated. The dynamic stress of the mooring line based on the data collection by the load cell is utilized in order to estimate the fatigue damage by means of the Rainflow counting method and a method based on fitting of probabilistic models to the stress cycle histograms. The peaks and valleys of the stress time histories of the mooring line are determined by using peaks prominence detection. The time series of the stress in the mooring line together with the identified peaks and valleys for each ice manage scheme are illustrated in figure 31.

(a) Case 1: Square updrift scheme   **(b) Case 2: Round circle scheme**

(c) Case 3: Circle updrift tracks   **(d) Case 4: Linear updrift track**

Figure 31. Stress Ranges from Peaks and Valley of Mooring Chain

After that, the peaks and valley of the tension stress in the mooring line are adopted to determine the stress range by using the Rainflow counting algorithm. For the probabilistic

36

approach, the stress ranges from the Rainflow counting algorithm are applied in order to be fitted with various probabilistic models. Subsequently, the fitted models can be applied for direct estimation of fatigue damage based on closed form analytical expressions. Various probabilistic models are applied in order to fit to the stress range data. Subsequently, it is found that three types with Lognormal, Exponential and Weibull distribution provides the appropriate fitting of the stress ranges from Rainflow counting algorithm. The types of probability model for the stress range in the mooring line is similar to the stress range of ice load on the ship hull, which can be present with the Exponential and Weibull distribution (Chai et al., 2018b). The examples of the probability plots for case 1: square updrift pattern are illustrated in the figure 32. The probability density functions, PDFs of stress range with Lognormal, Exponential and Weibull distribution for each case IM operation scheme are demonstrated in figure 33.
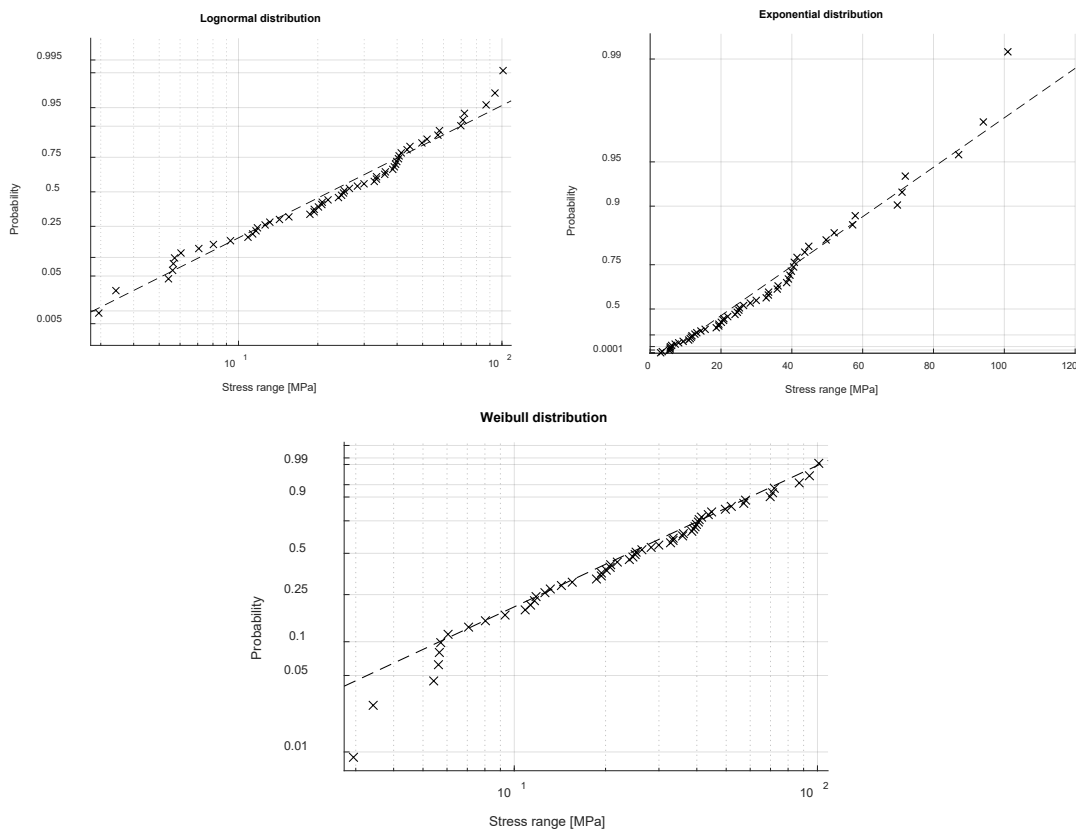
Figure 32. Example of PDF fitting in probability paper of the empirical stress ranges for the mooring chain (Case 1: Square updrift scheme)
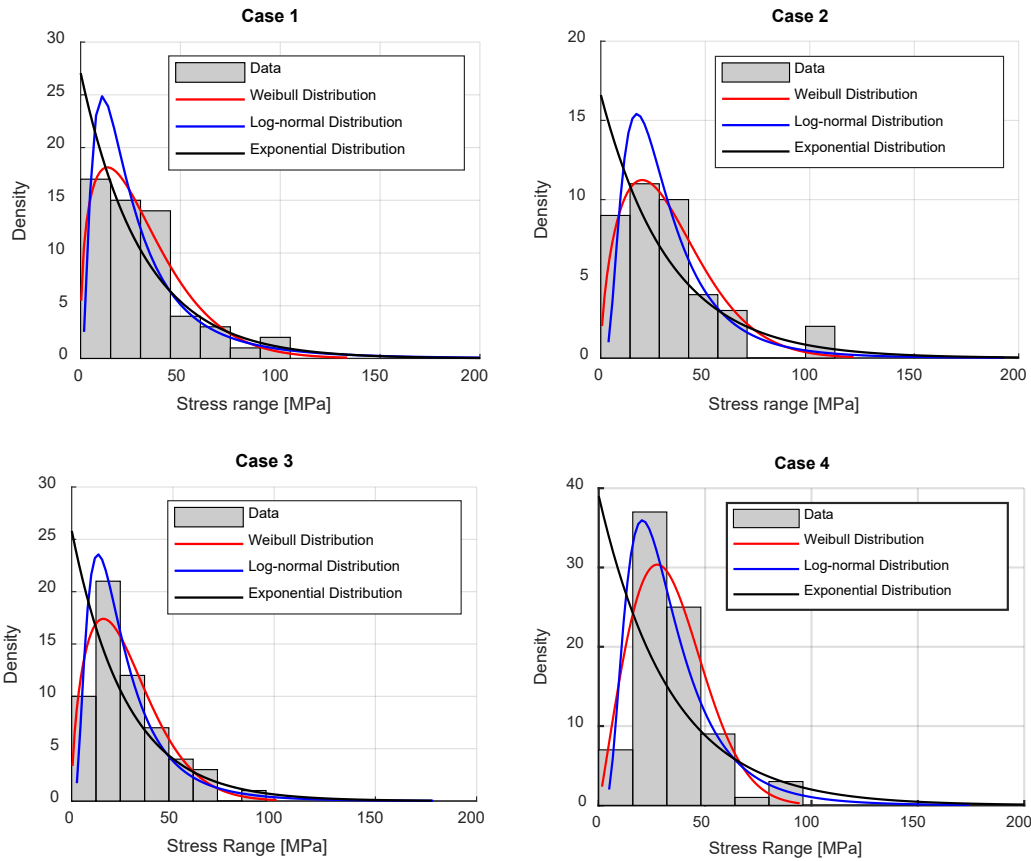
Figure 33. PDFs of the mooring chain stress ranges for each ice management scheme based on fitting oto data from full-scale measurements

5. Discussion

5.1 Estimation of ice loading based on the ice resistance method

The mooring tension for the ship during station-keeping in drifting ice can be estimated in a quite simple manner based on the ice resistance formulation (Riska, 1997). However, estimation based on this approach does not take into account the effects of the different ice management schemes. Still, the uncertainty associated with the calculated mooring load can be quantified by means of the direct measurements of the ice thickness and ice drift speed in combination with statistical models of the other relevant parameters in the load formula. The results are shown in Figure 34. The mean value of the measured ice loads for cases 2 to 4 are lower than the calculated ones, while the opposite is observed for case 1.

The difference between the values of the measured versus calculated loads is a measure of the efficiency of each ice management scheme. The maximum efficiency is observed for case 3 which corresponds to the circular updrift pattern. This is followed by case 4 and 2, respectively. For case 1, the station for observation of the ice thickness is located at a certain distance from the full-scale test site. For this case the ice drift speed has the highest value. Furthermore, the ice concentration is approximate 9-10. Therefore, accumulation of level ice

pieces can take place such that an ice ridge is formed before reaching the MV vessel. In turn, this will increase the global ice load, and this implies that the measured ice load is higher than the calculated one for case 1.
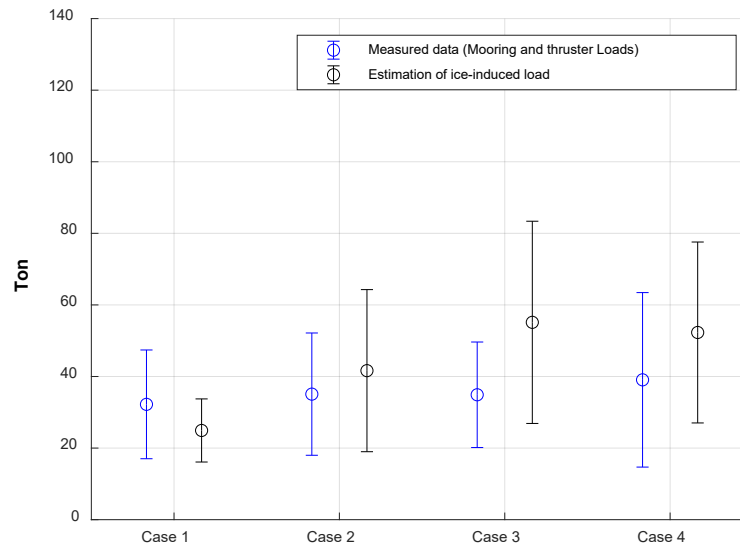
Figure 34. Comparison of the mean values and standard deviation for the measured load versus the calculated load based on the ice resistance method for each IM scheme

5.2 Extreme load prediction

According to the offshore standard for general marine operation by DNV-OS-H101(Veritas), the accepted return period for design purposes depends upon the reference period for the field operation. For the present experiment, a one-week operation was considered for the full-scale test (not including installation, dynamic positioning test and other tests). The minimum accepted design return period for a one-week operation is three months, which is used for the purpose of short-term extreme value analysis. However, it should also be kept in mind that the present offshore standard was originally developed for operations in open water.

For a three-month return period and with a reduction factor, R, corresponding to an operation frequency equal to 0.375, the comparison of extreme mooring forces for the POT, ACER, and BM methods as well as the extreme value of the ice resistance method is demonstrated in figure 35. The extreme values of the ice resistance method are estimated, based on the peak over threshold method. However, the extreme value of the ice resistance method does not take into account the ice management effect. All results of the extreme value analysis for each case are higher than the capacity of the load cell (150 tons) and the minimum breaking load, (MBL = 223 ton) of the steel wire. Therefore, the thruster is required to support the mooring line for the safe operation when the mooring load reached a level of 100 tons. Furthermore, the extreme values of the ice resistance method are higher than the minimum breaking load of the mooring chain (MBL, 611ton). This implied that the operation of the

vessels in cases 3 and 4 without the ice management operation can provide the possibility of exceeding the minimum breaking load for the mooring change.
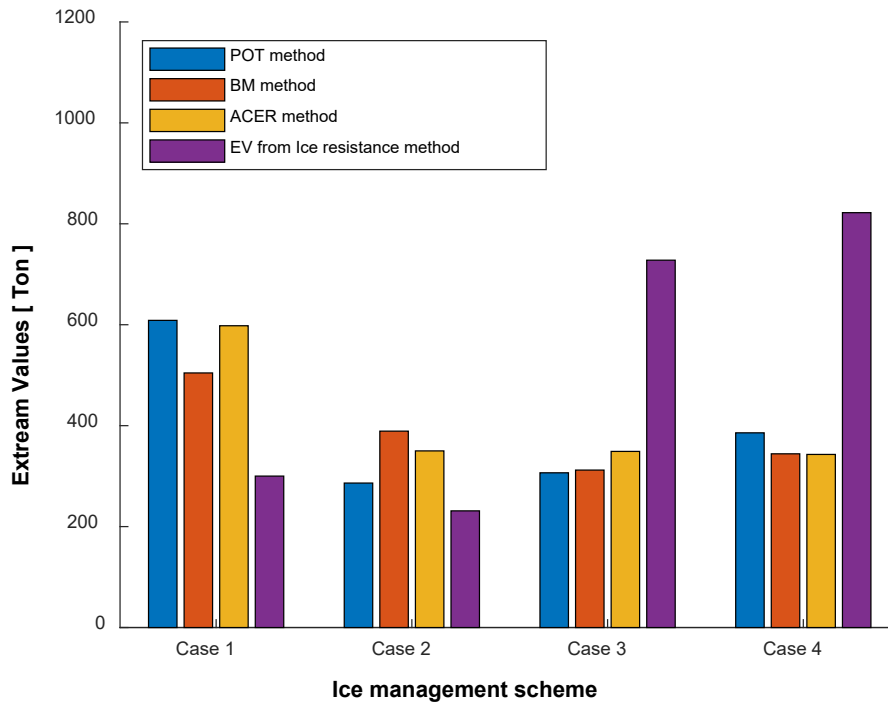
Figure 35. the comparison of extreme mooring forces for each ice manage scheme.

In this present study, the efficiency of the different ice management schemes was quantified by considering the ratio between the ice thickness/draft and the extreme mooring loads as illustrated in figure 36a. It is found that case 1: the square updrift pattern and case 2: the round circle pattern implies the lowest efficiencies among the IM schemes because it provides the lowest distance of the icebreaker track in front of the vessel. The highest efficiency among the ice management schemes seems to occur for case 3: the circular updrift pattern, following by case 4: the linear updrift pattern and case 1: Square updraft pattern respectively. These schemes provide sharp traces of the icebreaker, which serves to cut the sea ice in the updrift direction as shown in Figure 20. For the linear updrift pattern (case 4), the tracks of the ice breaker are parallel to ice drift direction in front of the supply vessel, which can create an ice channel. It is more efficient than case 1, i.e. the square updrift pattern. For this case, the icebreaker is cutting the sea ice in a direction which is perpendicular to the longitudinal orientation of the supply vessel. The center of the broken ice sheet can then drift towards the supply vessel. This can generate higher ice loads, which implies a lower efficiency for this ice management scheme.
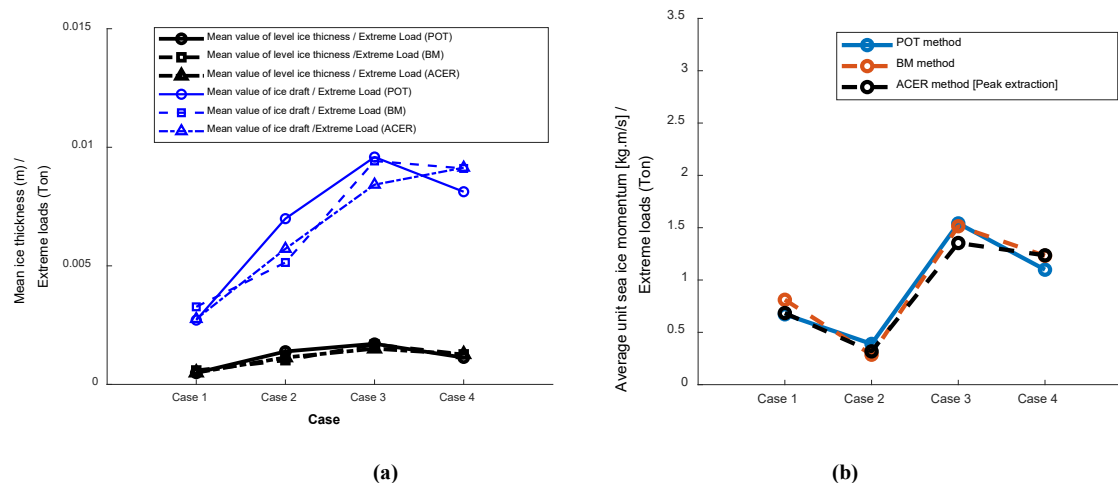
Figure 36. a) Efficiency of ice management operations by consideration of extreme loads and ice thickness/draft for level ice and ridges, respectively, b) Efficiency of ice management operations by consideration of average unit sea ice momentum.

The major factors that influence the IM operations are the level ice thickness, ice draft, ice drift speed and capacity of the icebreaker (El Bakkay et al., 2014). Regarding the ice conditions, the ice thickness/draft and ice drift speed during the full-scale tests can be considered for calculation of the average unit ice momentum in order to estimate the efficiency of the IM operations as demonstrated in figure 36b. The unit momentum is calculated from the average mass corresponding to the ice thickness and ice draft multiplied by the average ice drift speed.

It is found that the highest efficiency of the IM operations by considering the average unit ice momentum occurs for case 3: the circular updrift pattern, which is the same observation regarding the relative efficiency of this IM operation as obtained by considering only the ice thickness/draft. However, the efficiency for case 1: the square updrift pattern increases when the momentum is considered because the sea ice drifts with the highest speed for this case (which increases the average sea ice momentum). The lowest efficiency among the IM operations for the momentum criterion occurred for case 2, which is a little bit different from the result obtained by considering only the ice thickness/draft.

The track of the icebreaker for case 2: round circular pattern covers the whole area around the supply vessel, *MV*. Therefore, the efficiency of the ice breaking process in the upstream direction of the ice drift is reduced due to the short traveling distance for which the sea ice is cut. This tends to reduce the efficiency of the IM operation. However, the round circular pattern is of advantage for regions where the ice drift directions are changing rapidly.

The short-term extreme mooring loads estimated by the POT, ACER and BM methods for each IM scheme are normalized by the maximum observed mooring load as illustrated in figure 37. The maximum normalized values were observed for case 1: square updrift pattern which resulted in 3.6, 3.0 and 3.5 for the POT, ACER and BM methods, respectively. The normalization values are approximately 2.4 - 4.0 for the ice resistance method. Typically, the maximum loads from the simulations of severe environmental conditions are utilized in order to design the mooring system. The results of the normalization implies that there will be a significant increase of the long-term extreme values as compared to the maximum loads observed during short-term operations.
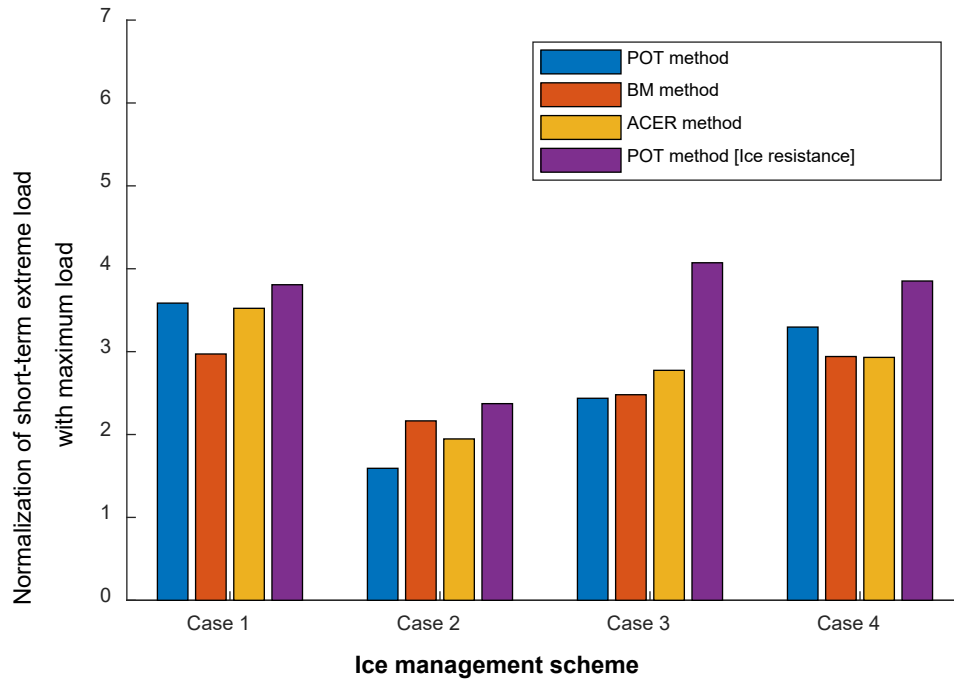
Figure 37. Normalization of extrapolated extreme values with maximum observed force during the tests.

Typically, there are several international standards for mooring design such as DNVGL(DNVGL, 2015), GL Noble Denton(Denton, 2013), American Bureau of Shipping (ABS)(ABS, 2018), Bureau Veritas(Veritas, 2005), etc. The safety factors in the international design standards are introduced in order to cover the uncertainty related to the estimated extreme loads and the structural resistance.

In this study, the safety factors are quantified in terms of the reserve strength capacity, calculated as the ratio between the minimum breaking loads, (MBL = 611 ton) of the main mooing chain (76mm type R4) and extreme mooring loading. The reserve strength of the mooring line is approximately 1.75 (MBL, 611ton / maximum extreme mooring load, 350 ton) for cases 2, 3 and 4. Whereas, the research strength is approximately equal to 1.0 for case 1: square updrift pattern, which has the low efficiency of the ice management. It is found that the reserve strength capacity of the main mooring chain is slightly lower than safety factors required by some relevant design standards i.e. DNVGL (S.F. = 1.9), ABS (S.F. = 2.25), GL Noble Denton (S.F. = 1.67), Bureau Veritas (S.F. = 1.67). For longer return periods (e.g. 1-year), this implies that stronger mooring lines should be employed. Moreover, the mooring systems also has a weak link at the load cell and a safety wire, which is able to disconnect in the case of an uncontrollable situation. This also enhances the degree of safety associated with the operation. Noticeably, the extreme value analysis is essential in the context of mooring system design in order to predict the highest loading that the system will experience during the operation.

5.3 Fatigue assessment of mooring lines

The probabilistic models are substituted in equation 34 in order to estimate the fatigue damage for each case. The results from the probabilistic approach as compared to the Rainflow counting method are shown in Figure 38. The overall trend seems to be that fitting by the Weibull

42

distribution provides fatigue damage estimates that are in best agreement with those from the Rainflow counting method. The highest fatigue damages take place at the Lognormal distribution following by Exponential distribution and Weibull distribution, respectively

Case 3: the circular updrift pattern and case 2: the round circle pattern provides the lowest magnitudes of the short-term fatigue damage. Systematic application of circular patterns during the ice management operations in order to protect a stationary vessel seems to be more efficient than application of systematic linear patterns.
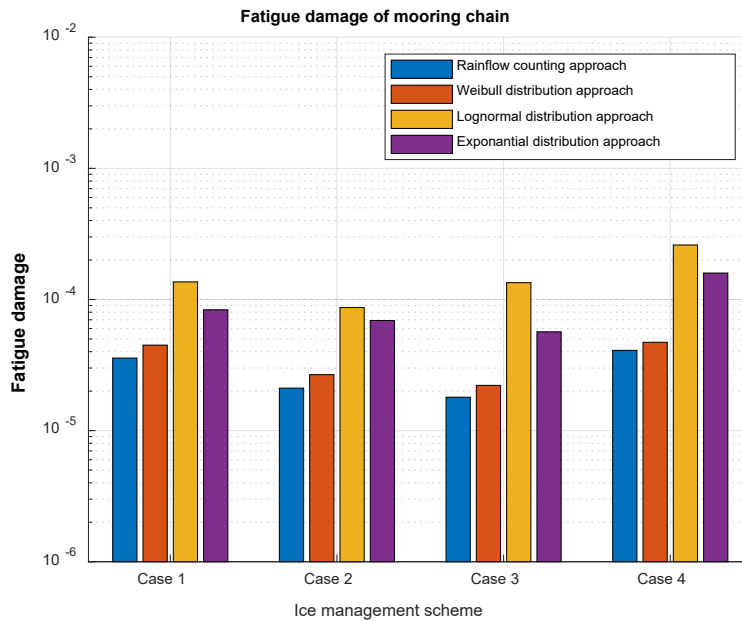
Figure 38. Comparison of estimated fatigue damage based on Rainflow counting versus fitting by means of different PDF models

6. Conclusions

6.1 Estimation of the ice loading based on the ice resistance method

The ice resistance method can be applied to estimate the global ice load that is acting on the mooring systems if the effects of ice management are disregarded. Therefore, it can be applied as the reference to identify the efficiency of a given IM operation by comparison with the measured mooring load for the supply vessel. Furthermore, the following is observed

- The uncertainty associated with the calculated the ice loading is due to the variability of the mechanical characteristics of the sea ice as well as variation of the ice thickness and ice drift speed.
- The highest efficiency of the different ice management schemes (which is observed by comparison with loads estimated by means of the ice resistance method), takes place for case 3: the circular updrift pattern.

6.2 Extreme value estimation

Short-term extreme value analysis of mooring loads obtained from full-scale measurements for different ice management schemes is performed. The associated extreme mooring loads are estimated in relation to four different ice management schemes which correspond to the square updrift, the round circle, the circular updrift and the linear updrift patterns. The tension in the mooring line during the full-scale experiment was monitored by a load cell and the measurements were recorded. The peaks loads from the resulting time series of the mooring load are analyzed in the present study by means of the POT, the ACER and the BM methods in order to estimate the statistical properties of the corresponding short-term extreme mooring loads.

- The results of the analysis are quite sensitive to the threshold value which is applied for the POT and to the width of the time window which is applied for the BM method.
- The extreme mooring loads, which are estimated by the three methods for a three-month return period in combination with a reduction factor, R, due to operation frequency which is equal to 0.375, agree quite well.
- The maximum difference between the results obtained by the three methods is about 20 percent. The uncertainty associated with the extreme value distribution is mainly due to the variation of the peaks of the mooring loads (which also correspond to the global ice loads on the supply vessel, MV).
- The highest efficiency among of the different ice management schemes is observed for case 3: the circular updrift pattern. This is followed by case 4: the linear updrift pattern. The lowest efficiency occurs for case 1: the square updrift tracks.

In general, analysis of extreme mooring loads is essential for the purpose of mooring system design in order to ensure adequate safety and integrity, not the least for temporary operations in the Arctic

6.3 Fatigue assessment

Probabilistic models are fitted to the empirical distributions of the mooring line stress ranges for each ice management scheme based on the full-scale data. Short-team fatigue damage evaluated by means of Rainflow counting approach versus fitted probabilistic models for the stress ranges are investigated.

- For the fatigue assessment based on fitted models, the stress ranges in the tail region play a dominant role in relation to estimation of fatigue damage, even though the number of stress ranges in this region is relatively small.

- Representing the stress ranges by means of the Weibull distribution resulted in fatigue damage estimates which are in best agreement with those obtained by application of the Rainflow counting approach.

- Representing the stress ranges by means of the Lognormal and Exponential distributions resulted in somewhat higher fatigue damage estimates than those from the Rainflow counting approach.

- Among the different ice management schemes, the circular updrift pattern provided the lowest magnitude of the estimated fatigue damage.

- Ice management operations applying circular patterns seem to be more efficient than the systematic linear patterns.

As part of future research, additional full-scale tests will clearly be valuable in order to enhance the precision associated both with estimation of extreme values and fatigue damage.

7. Acknowledgments

8. References

ABS, 2018. Guide for Position Mooring Systems. American Bureau of Shipping Incorporated by Act of Legislature of the State of New York.

ACER, 2013. The ACER user resources: https://folk.ntnu.no/arvidn/ACER/

API, R.S., 1996. Recommended practice for design and analysis of stationkeeping systems for floating structures. American Petroleum Institute.

Chai, W., Leira, B.J., Naess, A., 2018a. Probabilistic methods for estimation of the extreme value statistics of ship ice loads. Cold Regions Science and Technology 146, 87-97.

Chai, W., Leira, B.J., Naess, A., 2018b. Short-term extreme ice loads prediction and fatigue damage evaluation for an icebreaker. Ships and Offshore Structures 13 (sup1), 127-137.

Chai, W., Leira, B.J., Sinsabvarodom, C., Shi, W., 2021. Estimation of Ice Conditions Along the Northern Sea Route. Springer Singapore, Singapore, pp. 397-408.

Denton, G.N., 2013. Technical policy board guidelines for moorings, GL noble denton 0032/ND. GL Noble Denton.

DNVGL, 2015. DNVGL-OS-E301 Position Mooring. DNV GL, Oslo.

El Bakkay, B., Coche, E., Riska, K., 2014. Efficiency of Ice Management for Arctic Offshore Operations. (45561), V010T007A041.

Erceg, S., Ehlers, S., 2017. Semi-empirical level ice resistance prediction methods. Ship Technology Research 64 (1), 1-14.

Far, S.S., Wahab, A.K.A., 2016. Evaluation of peaks-over-threshold method. Ocean Science Discussions, 1-25.

Fenz, D., Younan, A., Piercey, G., Barrett, J., Ralph, F., Jordaan, I., 2018. Field measurement of the reduction in local pressure from ice management. Cold Regions Science and Technology 156, 75-87.

Goda, Y., 1989. On the methodology of selecting design wave height, Coastal Engineering 1988, pp. 899-913.

Gürtner, A., Baardson, B.H.H., Kaasa, G.-O., Lundin, E., 2012. Aspects of importance related to Arctic DP operations, International Conference on Offshore Mechanics and Arctic Engineering. American Society of Mechanical Engineers, pp. 617-623.

Hahn, M., Dankowski, H., Ehlers, S., Erceg, S., Rung, T., Huisman, M., Sjöblom, H., Leira, B.J., Chai, W., 2017. Numerical Prediction of Ship-Ice Interaction: A Project Presentation, ASME 2017 36th International Conference on Ocean, Offshore and Arctic Engineering.

Hamilton, J., Holub, C., Blunt, J., Mitchell, D., Kokkinis, T., 2011. Ice management for support of arctic floating operations, OTC Arctic Technology Conference. Offshore Technology Conference.

Haugen, J., Imsland, L., Løset, S., Skjetne, R., 2011. Ice Observer System For Ice Management Operations, The Twenty-first International Offshore and Polar Engineering Conference. International Society of Offshore and Polar Engineers, Maui, Hawaii, USA, p. 8.

Hopkins, M.A., Hibler III, W., Flato, G., 1991. On the numerical simulation of the sea ice ridging process. Journal of Geophysical Research: Oceans 96 (C3), 4809-4820.

Ionov, B., 1988. Ice resistance and its composition. Arctic and Antarctic Research Institute, Gidrometeoizdat, Leningrad.

ISO, B., 2010. 19906: 2010. Petroleum and natural gas industries–Arctic offshore structures.
Kämäräinen, J., 1993. Evaluation of ship ice resistance calculation methods.

Kjøl, A., Liferov, P., Almkvist, E., Lindvall, J.K., McKeever, T., 2018. Station-keeping trials in ice: Marine spread, ASME 2018 37th International Conference on Ocean, Offshore and Arctic Engineering. American Society of Mechanical Engineers, pp. V008T007A023-V008T007A023.

Kujala, P., 1996. Semi-empirical evaluation of long term ice loads on a ship hull. Marine Structures 9 (9), 849-871.

Kuuliala, L., Kujala, P., Suominen, M., Montewka, J., 2017. Estimating operability of ships in ridged ice fields. Cold Regions Science and Technology 135, 51-61.

Leira, B.J., 2016. Reliability updating based on monitoring of structural response parameters. Reliability Engineering & System Safety 155, 212-223.

Leppäranta, M., 2011. The drift of sea ice. Springer Science & Business Media.

Li, F., Suominen, M., Lu, L., Kujala, P., Taylor, R., 2021. A probabilistic method for long-term estimation of ice loads on ship hull. Structural Safety 93, 102130.

Liferov, P., McKeever, T., Scibilia, F., Teigen, S.H., Kjøl, A., Almkvist, E., Lindvall, J.K., 2018. Station-keeping trials in ice: Project overview, ASME 2018 37th International Conference on Ocean, Offshore and Arctic Engineering. American Society of Mechanical Engineers, pp. V008T007A029.

Lindquist, A., 1989. Straightforward method for calculation of ice resistance of ships. POAC'89.

Matsuishi, M., Endo, T., 1968. Fatigue of metals subjected to varying stress. Japan Society of Mechanical Engineers, Fukuoka, Japan 68 (2), 37-40.

Mellor, M., 1980. Ship resistance in thick brash ice. Cold Regions Science and Technology 3 (4), 305-321.

Naess, A., Gaidai, O., 2009. Estimation of extreme values from sampled time series. Structural Safety 31 (4), 325-334.

Naess, A., Gaidai, O., Karpa, O., 2013. Estimation of extreme values by the average conditional exceedance rate method. Journal of Probability and Statistics 2013.

Naess, A.A., 1985. Fatigue handbook: offshore steel structures. Tapir.

Neville, M., Almkvist, E., Scibilia, F., Lindvall, J.K., Liferov, P., 2018. Station-keeping trials in ice: Overview of ice management support, ASME 2018 37th International Conference on Ocean, Offshore and Arctic Engineering. American Society of Mechanical Engineers, pp. V008T007A027-V008T007A027.

Neville, M.A., Scibilia, F., Martin, E.H., 2016. Physical Ice Management Operations - Field Trials and Numerical Modeling, Arctic Technology Conference. Offshore Technology Conference, St. John's, Newfoundland and Labrador, Canada, p. 19.

Nyseth, H., Hansson, A., Iseskär, J.J., 2018. Station Keeping Trials in Ice: Ice Load Monitoring System, ASME 2018 37th International Conference on Ocean, Offshore and Arctic Engineering. American Society of Mechanical Engineers, pp. V008T007A031-V008T007A031.

Riska, K., 1997. Performance of merchant vessels in ice in the Baltic. Sjöfartsverket.

Riska, K., 2011. Design of ice breaking ships. Course material NTNU 114.

Ronkainen, I., Lehtiranta, J., Lensu, M., Rinne, E., Haapala, J., Haas, C., 2018. Interannual sea ice thickness variability in the Bay of Bothnia. The Cryosphere 12, 3459-3476.

Serre, N., Kerkeni, S., Sapelnikov, D., Akuetevi, C., Sukhorukov, S., Guo, F., Metrikin, I., Liferov, P., 2018. Station-Keeping Trials in Ice: Numerical Modelling, ASME 2018 37th International Conference on Ocean, Offshore and Arctic Engineering.

Sinsabvarodom, C., Chai, W., Leira, B.J., Høyland, K.V., Naess, A., 2019. Probabilistic Assessment of Ice Rose Diagrams for Ice Drift in the Beaufort Sea. Proceedings of the 25th International Conference on Port and Ocean Engineering under Arctic Conditions.

Sinsabvarodom, C., Chai, W., Leira, B.J., Høyland, K.V., Naess, A., 2020a. Uncertainty assessments of structural loading due to first year ice based on the ISO standard by using Monte-Carlo simulation. Ocean Engineering 198, 106935.

Sinsabvarodom, C., Leira, B.J., Chai, W., Naess, A., 2020b. Extreme Value Estimation of Mooring Loads Based on Station-Keeping Trials in Ice, ASME 2020 39th International Conference on Ocean, Offshore and Arctic Engineering. American Society of Mechanical Engineers.

Spreen, G., Kwok, R., Menemenlis, D., 2011. Trends in Arctic sea ice drift and role of wind forcing: 1992–2009. Geophysical Research Letters 38 (19).

Suyuthi, A., Leira, B.J., Riska, K., 2012a. Non Parametric Probabilistic Approach of Ice Load Peaks on Ship Hulls, ASME 2012 31st International Conference on Ocean, Offshore and Arctic Engineering, pp. 415-423.

Suyuthi, A., Leira, B.J., Riska, K., 2012b. Short term extreme statistics of local ice loads on ship hulls. Cold Regions Science and Technology 82, 130-143.

Teigen, S.H., Lindvall, J.K., Samardzija, I., Hansen, R.I., 2018. Station-keeping trials in ice: Ice and metocean conditions, ASME 2018 37th International Conference on Ocean, Offshore and Arctic Engineering. American Society of Mechanical Engineers, pp. V008T007A030-V008T007A030.

Veritas, B., 2005. Classification of Mooring Systems for Permanent and Mobile Offshore Units. Rule Note NR 493.

Veritas, D.N., DNV-OS-H101 Marine Operations, General, no. October 2011. Available: h https://rules. dnvgl. com/docs/pdf/DNV/codes/docs/2011-10/Os-H101.

Veritas, D.N., 2010. Offshore standard DNV-OS-E301 position mooring. Det Norske Veritas: Høvik, Norway.

Wang, Q., Zong, Z., Lu, P., Zhang, G., Li, Z., 2021. Probabilistic estimation of level ice resistance on ships based on sea ice properties measured along summer Arctic cruise paths. Cold Regions Science and Technology 189, 103336.

Yulmetov, R., Marchenko, A., Løset, S., 2016. Iceberg and sea ice drift tracking and analysis off north-east Greenland. Ocean Engineering 123, 223-237.